RADAR: THE CASSINI TITAN RADAR MAPPER

C. ELACHI[1,†], M. D. ALLISON[2], L. BORGARELLI[3], P. ENCRENAZ[4], E. IM[1], M. A. JANSSEN[1], W. T. K. JOHNSON[1], R. L. KIRK[5], R. D. LORENZ[6], J. I. LUNINE[6], D. O. MUHLEMAN[7], S. J. OSTRO[1], G. PICARDI[8], F. POSA[9], C. G. RAPLEY[10], L. E. ROTH[1], R. SEU[8], L. A. SODERBLOM[5], S. VETRELLA[11], S. D. WALL[1,*], C. A. WOOD[12] and H. A. ZEBKER[13]

[1]*Jet Propulsion Laboratory, California Institute of Technology, Pasadena, CA 91109, U.S.A.*
[2]*Goddard Institute for Space Studies, National Aeronautics and Space Administration, New York, NY 10025, U.S.A.*
[3]*Alenia Aerospazio, 00131 Rome, Italy*
[4]*Observatoire de Paris, 92195 Meudon, France*
[5]*U. S. Geological Survey, Flagstaff, AZ 86001, U.S.A.*
[6]*Lunar and Planetary Laboratory, University of Arizona, Tucson, AZ 85721, U.S.A.*
[7]*Division of Geological and Planetary Sciences, California Institute of Technology, Pasadena, CA 91125, U.S.A.*
[8]*Universitá La Sapienza, 00184 Rome, Italy*
[9]*Dip. Interateneo di Fisica, Politecnico di Bari, 70126 Bari, Italy*
[10]*British Antarctic Survey, CB3 0ET Cambridge, U.K.*
[11]*Facoltá di Ingegneria, 80125 Naples, Italy*
[12]*University of North Dakota, Grand Forks, ND 58202, U.S.A.*
[13]*Stanford University, Stanford, CA 94305, U.S.A.*
[*]*(Author for correspondence: E-mail address: stephen.d.wall@jpl.nasa.gov)*
[†]*RADAR Team Leader*

(Received 23 January 1998; Accepted in final form 12 March 1999)

Abstract. The Cassini RADAR instrument is a multimode 13.8 GHz multiple-beam sensor that can operate as a synthetic-aperture radar (SAR) imager, altimeter, scatterometer, and radiometer. The principal objective of the RADAR is to map the surface of Titan. This will be done in the imaging, scatterometer, and radiometer modes. The RADAR altimeter data will provide information on relative elevations in selected areas. Surfaces of the Saturn's icy satellites will be explored utilizing the RADAR radiometer and scatterometer modes. Saturn's atmosphere and rings will be probed in the radiometer mode only. The instrument is a joint development by JPL/NASA and ASI. The RADAR design features significant autonomy and data compression capabilities. It is expected that the instrument will detect surfaces with backscatter coefficient as low as −40 dB.

1. Introduction

The Cassini spacecraft, launched on October 15, 1997, carries a multimode Ku-band (13.8 GHz, λ2.17-cm) radar instrument (RADAR) designed to probe Titan's surface and other targets in the Saturn system. It is distinguished by a number of novel features which accommodate the large geometric variations in flyby trajectories and the wide range of uncertainty in surface properties, and which efficiently utilize

Space Science Reviews **xxx:** 1–40, 2004.

the limited spacecraft resources such as the data rates, the data volumes, and power. This article describes the science objectives, operational modes, and general design of the RADAR; the description given here updates the report published previously (Elachi *et al*., 1991).

The RADAR will investigate the surface of Titan using all four of its operational modes—imaging, altimetry, scatterometry, and radiometry. The radiometry and scatterometry will also be used to investigate other targets. The utility of radar imaging of solar-system objects, inaccessible to remote sensing at visible wavelengths has been demonstrated most dramatically by the success of the Magellan radar experiment at Venus (Johnson, 1991; Pettengill *et al*., 1991; Saunders *et al*., 1992). It has been known since the early 1960s (e.g. Pettengill *et al*., 1962) that the cloud-shrouded surface of Venus is solid. The correspondence in the radar cross-sections between Venus and the Moon, Mars, and Mercury (see, e.g. Ostro, 1993) indicated a gross similarity—both compositional and morphological—of Venus' surface to the surfaces of the inner planets. The Arecibo and Goldstone radars had produced impressive images of the part of Venus that faces the Earth when the two planets are closest and hence when Venus radar echoes are strongest (see, e.g. Campbell *et al*., 1983). Thus, even prior to the launch of the Magellan mission (and the Pioneer Venus and Venera 15/16 missions before) the expected return signal was fairly well understood and the results of the imaging operations anticipated. That situation does not prevail in the case of Titan, though some globally averaged radar reflectivity information exists.

Historically, the telescopic appearance of Titan has been compared to that of Mars and ascribed to the same physical causes. In the words of the discoverer of the atmosphere on Titan (Kuiper, 1944), "the color of Titan is orange, in marked contrast to Saturn and its other satellites or with Jupiter and its satellites. It seems likely that the color is due to the action of the atmosphere on the surface itself, analogous to the oxidation supposed to be responsible for the orange color of Mars." The Voyager images confirmed that the ball of Titan was indeed orange but the color has been attributed to the suspended products of the photo- and radiation-induced dissociation of atmospheric methane. As far-fetched as the idea of Titan made of iron oxides may seem, it was justified by the density estimates current in Kuiper's time, which made Titan even denser than the Moon (see Table 2 in Kuiper, 1944). The post-Voyager value of Titan's density, 1.88 g cm^{-3} (Tyler *et al*., 1981; Lindal *et al*., 1983), allows for a silicate abundance comparable to or less than that of ices and organics together. The suspended aerosol particles represent one end state of the photolysis of methane, which also results in the escape of hydrogen from the planet. Post-Voyager estimates put the loss time of all the atmospheric methane at about 1% of the age of the solar system. To account for the supply of methane in the atmosphere, a family of models proposed to date require (or admit) the existence on the Titan's surface of a massive, perhaps global, methane reservoir, along with ethane, propane, and other hydrocarbons (Lunine *et al*., 1983; Dubouloz *et al*., 1989; Lunine and Rizk, 1989; Lunine, 1993). But the 1.7 dielectric

constant of most light hydrocarbons at 90 K (e.g. Straty and Goodwin, 1973; Sen *et al*., 1992), implies that the reflectivity of an ethane–methane mixture is equal to 0.02. Titan, if it were indeed covered by a smooth, deep ethane–methane ocean, would generate a weak, specular, longitude-independent radar echo. The results of the λ3.5-cm Goldstone/VLA Titan radar experiments indicate otherwise: Titan has been found to return a relatively strong, diffuse, and longitude-dependent echo (Muhleman *et al*., 1990, 1992, 1993, 1995). On the average, Titan behaves in a manner similar to a Lambertian scatterer, with echoes returned by nearly the entire Earth-facing hemisphere. The radar cross-section peaks around longitude 90°W (Figure 16 in Muhleman *et al*., 1995), suggesting that a sizeable segment of the Titan's leading hemisphere is free of liquid hydrocarbons. Measurements of the λ3.5-cm radio emission from Titan have yielded emissivity of 0.88 ± 0.03; this corresponds to materials with the dielectric constant of 2.9 ± 0.6 (Grossman and Muhleman, 1992). Taken alone, the λ3.5-cm reflectivity and the angular scattering behavior of Titan are closer to those of Callisto than other radar-studied targets (Figure 17 in Muhleman *et al*., 1995). When the circular polarization ratio (i.e., the ratio of the same-sense to the opposite-sense circularly polarized cross-sections), μ_c, is also taken into account, the main-belt asteroid 4 Vesta, believed to have basaltic crust, emerges as the closest radar analog to Titan (Mitchell *et al*., 1996; Figure 1). Kuiper erred in assessing the reasons for the optical appearance of Titan, but he seems to have anticipated Titan's radar properties—perhaps for wrong reasons also. Contamination by silicates may be responsible for the Vesta-like radar characteristics of Titan, as might coating by solid photolytic debris. (For a review of the dielectric properties of higher hydrocarbons, see Thomson and Squyres, 1990.) As a consequence of the Goldstone/VLA measurements a global ocean on Titan should be seen as improbable, but discrete ethane–methane lakes or inland seas are by no means ruled out. Telescopic observations in the 0.9, 1.1, 1.3, 1.6, and 2.0 μm methane windows confirm the apparent heterogeneity of Titan's surface (Griffith *et al*., 1991; Griffith, 1993; Lemmon *et al*., 1993, 1995). Regional albedoes might be consistent with the presence of the water/ammonia ice and of an unspecified dark material—possibly the debris left behind by the methane photochemistry. The 0.9 and 1.1 μm Hubble Space Telescope maps of Titan (Smith and Lemmon, 1993; Smith *et al*., 1994, 1996) show a feature with an albedo of about 8% above the background, centered at the longitude of 110°W, and covering 10^7 km^2 (i.e. 10% of the total area of Titan). The feature is located on the surface itself and coincides with the source region of the strong Goldstone/VLA radar echoes (Figure 8 in Smith *et al*., 1995). The demise of the notion of a global ocean makes the case for orbital imaging of Titan even more compelling. Given the contrast between the higher-permittivity "bedrock" and the lower-permittivity liquid hydrocarbons, detection of ethane–methane lakes in the RADAR data should be a straightforward matter.

The bright IR/radar feature has been referred to as a "continent," but its actual physical nature is unknown. Neither an impact-related excavation of cleaner ice nor a volcanic resurfacing of the (presumably) tholin-coated bedrock are deemed to be

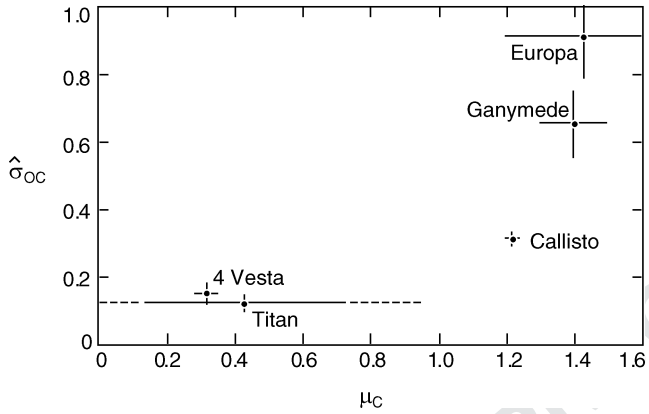

Figure 1. The λ3.5-cm opposite-sense radar albedo, σ_{oc}, vs. the circular polarization ratio, μ_c, for the Moon, Titan, 4 Vesta, Callisto, Europa, and Ganymede. *Data sources*: The Moon, Table 3 in Harmon and Ostro (1985) and Table 1 in Pettengill (1978); Vesta, Table 7 and Figure 11 in Mitchell *et al*. (1996); Callisto, Europa and Ganymede, Table 8 in Ostro *et al*. (1992). The value for the mean cross-section of Titan is from Muhleman *et al*. (1995), p. 369. The error bar on μ_c for Titan was computed from data in Table 1 in Muhleman *et al*. (1995). Ganymede and Europa are included for comparison, as the objects with the most extreme radar properties.

the likely generation mechanism of the feature (Smith *et al*., 1996). Since methane precipitation is possible on Titan (Toon *et al*., 1988), and the associated limitations on the erosion rates are at least qualitatively understood (Lorenz, 1995a; Lorenz and Lunine, 1996), the bright feature has tentatively been identified as a topographic high exposed to the cleansing effect of methane rainfall (Smith *et al*., 1996). Since that cleansing would wash away tholin deposits, the enhanced strength of the radar echo, returned presumably by clean (or cleaner) ice, could then be easily explained. The seasonal hemispheric brightness variability, the other telescopically observed phenomenon on Titan, is probably related to processes taking place well above the surface (Caldwell *et al*., 1992; Lorenz *et al*., 1997), and thus is of no immediate interest to RADAR.

2. Science Objectives

The overall science objectives of the Cassini mission include five Titan-specific objectives. Two of these—the determination of the physical state, topography, and composition of the Titan's surface; and the measurement of global temperatures and general circulation on Titan—constitute the overriding goal of the RADAR experiment. Whenever feasible, the RADAR will also conduct observations of the icy satellites, Saturn's rings, and Saturn itself. The Titan observations, however, constitute the highest scientific priority for the RADAR, and they drive its design.

2.1. TITAN

The general objective of the RADAR experiment is to carry out the first-order geological reconnaissance of Titan's surface and to derive a quantitative characterization of the surface. The approach is to use microwave radiation to penetrate opaque atmosphere, map the surface, and, combining RADAR data with the data from the Cassini optical remote sensing instruments, obtain a comprehensive understanding of Titan's physical condition. An important early objective is to acquire coverage of the Huygen's landing site. The purpose here is to give regional context to the data generated by the probe payload and particularly to the topography measurements from the probe's own (optical) imager and radar altimeter.

A global view of Titan and its geological and climatological history will result from mapping in all four RADAR modes. Special attention will be paid to the moon's cratering record. The crater size distribution, particularly as a function of elevation, will provide a constraint on the duration and extent of any episodes of atmospheric collapse (Engel *et al*., 1995). Crater morphology is an indicator of subsurface structure and, by implication, of Titan's thermal history. The likelihood of surface liquids suggests that there may be hydroblemes (seabed impact craters) and tsunami deposits. Although only a fraction—about 25%—of Titan's surface will be mapped in the SAR mode, the long, thin coverage swaths are an efficient means of establishing the crater distribution—a large impact crater is more likely to be cut by a long, thin swath than by a square patch of the same area (Lorenz, 1995b).

The polar regions of Titan are also important targets for RADAR SAR imaging. The polar climate may have experienced more variability than the global average. The reason for this is that Titan's obliquity is fractionally larger than the Earth's, and although its present atmosphere damps out seasonal changes, a thinner past atmosphere may have allowed the polar temperatures to swing widely. A recent re-analysis of Voyager IR data suggests that the poles may experience more precipitation than the equatorial regions, raising the likelihood of surface liquids and erosional features. The seasonal effects on the polar hazes (Samuelson *et al*., 1997) may also make these regions more difficult to observe at optical wavelengths. Q4

The RADAR altimetry data will provide information on relative elevations along portions of the suborbital tracks. The SAR and altimetry data will be examined to seek evidence for the effects of crustal processes such as viscous relaxation and cryovolcanism. Volumes of the cryovolcanic constructs identified in the altimetry data, may indirectly constrain Titan's hydrocarbon budget, while morphometry of erosional features may provide information about the rates at which volatiles are recycled.

The high-resolution (350–720 m) SAR images will permit identification of features and terrain types that will be observed in varying locations on Titan and in different viewing geometries. RADAR scatterometer data will reveal the backscatter efficiency versus incidence angle for a large fraction of Titan' surface, although

the spatial resolution may be coarse (as in the radiometer mode). Nonetheless, scatterometer data will constrain surface slope distribution and the density of the uppermost decimeter of the surface. Scatterometer data will also be most similar to the data taken with the upgraded Arecibo radar during the coming decade and therefore will allow Titan's global radar properties to be defined in detail.

In its radiometric mode, RADAR will produce thermal emission (brightness temperature) maps of essentially the entire surface of Titan. To this end, the spacecraft will be commanded to execute spiral scanning maneuvers. The spiral scanning will be expanded in targeted areas by rolling the spacecraft about the z-axis. The emissivity and the integrated reflectivity are complementary (but anti-correlated) quantities. Because the radar backscatter that is measured by the instrument is also related (although weakly) to the integrated reflectivity, the radiometer data may be expected to provide additional information on the nature of Titan's surface. The radiometric brightness temperature and its dependence on polarization and angle of incidence will be used to discriminate among surfaces of smooth and broken ice fields, liquid hydrocarbon lakes, and ice coated with organic precipitates from the atmosphere. Specifically, we will augment the interpretation of the active-modes RADAR data by constraining large-scale (10–30 km) surface composition from dielectric properties measured along radar tracks. Emissivity (as well as radar reflectivity) of a given substance is a strong function of the density; thus an emissivity map can be interpreted as a surface density map. We hope to discriminate between ice and snow or rock and soil in this way. A procedure which is being developed to interpret the RADAR radiometry data will also be used to model observations of comet Wirtanen with the Microwave Instrument for the Rosetta Orbiter (MIRO). Finally, taking advantage of the repeated opportunities to collect radiometer data over the entire disk of Titan, we will investigate global circulations and thermal transport by determining physical temperature contrasts between equator and poles, and between night and day.

The RADAR is a single-polarization instrument, but information about the polarization state of echoes is often needed to make unambiguous statements about physical properties. Arecibo's λ12.6-cm data will provide a very accurate curve of Titan's disk-integrated radar cross-section in two polarizations for subradar tracks near the equator (as well as nearly global maps with resolutions of order of several hundreds of kilometers). The availability of Cassini RADAR disk-integrated cross-sections will permit direct, model-independent calibration of Cassini and Arecibo data against each other, and also will define a solid boundary condition on models of the backscattering function's variation over the surface. Titan fills the RADAR center beam, at about a million kilometers, so disk-integrated measurements should be made no closer than that. At that distance, even a 1 s integration with the scatterometer will produce an echo much stronger than what Arecibo can obtain on any given date.

In order to make the results of the RADAR experiment easily accessible, we will devise means of placing the data in a consistent spatial framework in which

the individual datasets (SAR, thermal emission, and altimetry/scatterometry) will be combined with one another and with the optical remote sensing data. As part of this objective, we will construct a global geodetic control network for Titan. This is needed to compare the various types of observations, and it will allow determination of the spin pole direction and rotation period of Titan (cf. Hubbard *et al*., 1993; Lemmon *et al*., 1993, 1995). Cartographic products will be generated from individual observations, mosaics of like data, and composites of different, coregistered datasets. Digital maps in sinusoidal and oblique sinusoidal projections, and hardcopy products in conformal projections, will be produced at a range of scales, with appropriate divisions of the surface of Titan. Also, topographic mapping of Titan will be attempted by digital stereogrammetry (where overlapping SAR images are obtained with favorable geometry), and by radarclinometry (shape from shading in single images). Ganymede, which is similar in size to Titan and has been observed at resolutions comparable to those of the RADAR (Inge and Batson, 1992), provides the initial model for the Titan cartographic program.

2.2. Icy satellites

In general, the IR measurements of icy satellites are most sensitive to the conditions in the upper few centimeters of the surface. Measurements around all phase angles contain information to depths of up to several tens of centimeters, which can be retrieved in only a model-dependent way, e.g. on the assumption of constant density and thermal parameters over that depth. Measurements at microwave frequencies are sensitive to temperatures down to the depth of about 1 m if the ice is dense Q5 and several meters if the ice is under-dense. The thermal properties of the surface regolith, e.g. the ability to retain heat, may further be constrained by temperature measurements as a function of local time. Therefore an objective of the Cassini RADAR is to conduct radiometric observation of icy satellites during untargeted flybys at distances of less than about 100,000 km. Operations at closer ranges, when the satellite disk can be covered by a sufficient number of footprints, will give an opportunity to identify "hot spots" if there is cryovolcanic activity as is conceivable at least for Enceladus.

The Earth-based radar backscatter measurements in the outer solar system have been limited to the Galilean satellites and Titan (for a review, see Ostro, 1993). The RADAR scatterometry mode allows backscatter measurements on Saturn's icy satellites also. This can be seen from a simple comparison of the Cassini RADAR with the Goldstone radar—the least sensitive of the three Earth-based planetary radar systems (Goldstone, Goldstone/VLA, Arecibo). The RADAR's emitted power is about 10^{-4} of the power emitted by Goldstone, and the gain of the Cassini Orbiter High Gain Antenna (HGA) is about 10^{-5} of the gain of the Goldstone 70 m dish. The deficit of nine orders of magnitude can be compensated for by the fact that even during distant flybys (100,000 km) of icy satellites the RADAR is about 10^4 times closer to these targets than are the Earth-based radars. Taking into account the r^{-4}

dependence of the received power, the RADAR might thus be about 10^7 times more sensitive than the Goldstone system. As an example, the RADAR scatterometer can obtain a signal-to noise ratio equal to 2 (comparable to that obtained by the Goldstone/VLA observations of Titan; see Muhleman *et al*., 1990) by integrating only 1400 pulses from 500 km objects (Dione, Tethys) at a range of 300,000 km. Much higher signal-to-noise and spatially resolved measurements can be achieved at shorter ranges. Since radar cross-sections are equivalent to microwave albedoes, these measurements will complement the measurements of the visible and IR albedoes obtained by the Cassini optical remote sensing instruments. Furthermore, the RADAR scatterometer observations of icy satellites may be conducted at ranges too large to be useful to optical remote sensing. (Tour 18-5 offers 138 flybys of icy satellites at ranges from 100,000 to 300,000 km.) This would contribute to the optimal utilization of all available tour segments.

2.3. SATURN'S RINGS

Microwave flux due to the thermal emission by the rings particles and to scattering by the same particles of the emission from the deep atmosphere of Saturn will be sensed in the RADAR radiometer mode. Microwave emission from the ring particles uniquely probes through the mass of the particles because the λ2-cm wavelength penetration depth is of the order of 1 m. Thus, the RADAR radiometer presents the best way to measure the ice-to-dust ratio of the particles, as a function of radial distance from Saturn. Several radial scans of the ring system will be required during high-inclination Saturn passes.

2.4. SATURN

The deep subcloud region of Saturn is inaccessible to observation by means other than the measurement of thermal emission that originates in that region. The RADAR objective is to map variations in ammonia humidity in the subcloud region, which can be achieved through RADAR radiometer mapping. Ammonia is a tracer of atmospheric motions and provides unique insight into the dynamics of Saturn's atmosphere. Also, the radiometer provides a deeper, and hence complementary, weighting function to other Cassini instruments that operate at shorter wavelengths, and makes an essential contribution to the sounding of Saturn's atmosphere.

Microwave imaging of Saturn at centimeter wavelengths from the Very Large Array (VLA) (Grossman *et al*., 1989) reveals significant latitudinal structure, plausibly interpreted as a decrease in the ammonia vapor abundance at the cloud deck from equator to pole (Grossman, 1990). VLA images of Saturn are compromised, however, by the geometrical foreshortening of the polar region as well as the aperture synthesis and necessary 3 h integration of zonally smeared observations, and

are limited to a 2% variation in their dynamic range. Polar observations at a near-normal viewing angle by the Cassini RADAR radiometer can resolve the horizontal ammonia structure in the region of the Saturn polar hexagon (Allison *et al*., 1990) and with complementary mapping from low-inclination orbits potentially afford characterization of vertical variations apparent at differing emission angles. The further prospects for these observations would include their possible interpretation as tracer-maps of Saturn's "potential vorticity" distribution (cf. Allison *et al*., 1995).

High-inclination flybys will be required for polar imaging, low-inclination flybys for acquiring a full longitudinal image of the planet. To conduct radiometric observations, the preferred range of distances to Saturn is anticipated to be between about $5R_S$ and $15R_S$. It is also the objective of RADAR to obtain synoptic thermal-emission images of Saturn's disk. These images will be used to calibrate the radiometer for the Titan radiometric mapping.

3. Experiment Description

Since the RADAR will operate almost exclusively during close flybys of its targets, altitudes will change rapidly throughout the data collection periods. Under such conditions, operations in a multiplicity of modes are a necessity. The instrument was designed to incorporate four modes: imaging (either high- or low-resolution), altimetry, scatterometry, and radiometry. The basics of operations in these modes are outlined below; the system design considerations are summarized in Sections 4 and 5.

An optimum Titan flyby scenario, in which all RADAR modes are exercised and a maximum volume of data is collected, calls for about 10 h of uninterrupted operations. At 5 h away from the closest approach, the spacecraft is about 100,000 km from Titan (Figure 2). At that distance the RADAR is used in the radiometer-only mode. As the spacecraft approaches Titan, the remaining modes are activated; first scatterometry, followed by altimetry, and, finally, imaging. Upon receding

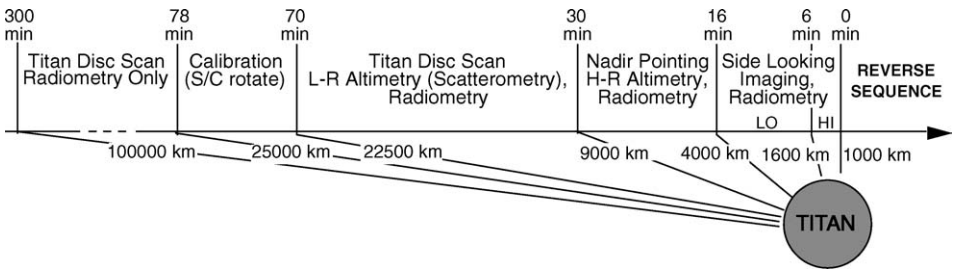

Figure 2. Sequence of the RADAR operational modes during a nominal Titan flyby. To the RADAR, the term "nominal" designates a flyby with the closest-approach altitude of 1,000 km.

TABLE I
Cassini RADAR Data Characteristics

	Altitude (km)	Incidence angle (°)	Resolution			NEσ_0 (at boresight) (dB)	Number of looks	Surface coverage (%)
			Azimuth (km)	Range (km)	Vertical (m)			
SAR								
High resolution	1,000–1,600	21–30	0.35–0.41	0.48–0.64	N/A	−28 to −21	2–3	≤1.1
Low resolution	1,600–4,000	15–28	0.41–0.72	0.48–2.70	N/A	−25 to −15	2–7	≤1.1
Altimeter	4,000–9,000	0	24–27	24–27	60	−3 to −35	16–36	N/A
Scatterometer	9,000–22,500	0–30	55–140	55–140	N/A	−4 to −36	N/A	20
Radiometer	1,000–100,000	0–80	6–600	6–600	N/A	N/A	N/A	40

N/A: Not available.

from Titan, the order of modes is reversed. A detailed description of the RADAR observational strategy is presented in Section 3.5 below.

3.1. IMAGING

The RADAR imaging mode provides low-to-high resolution synthetic aperture (SAR) images. The meaning of the terms "low" and "high" in the present context is clarified in Table I. Reference to appropriate analogs may be of further help. Q7 Thus, when considering the absolute pixel size, the low-resolution RADAR images will be comparable to the Venera-15/16 and Arecibo radar images of Venus, and the high-resolution RADAR images will be similar in resolution to the Mariner-9 optical images of Mars.

As the SAR data are being acquired, the spacecraft is pointed to the left or right of the nadir track. The way in which this off-nadir angle is varied is referred to as the look-angle profile, where look angle is the angle between boresight and nadir. Look angle is used to calculate the incidence angle—the angle between the antenna boresight and local surface normal. For typical natural surfaces, larger incidence angles tend to better reveal surface topography. From a mission standpoint, the profile of incidence (or look) angle used during SAR datataking is unconstrained except for limitations on spacecraft turning rates. One likely algorithm is to keep the largest incidence angle possible, consistent with a given received signal-to-noise ratio. This rule was followed during the primary mapping phase of the Magellan mission. An alternative philosophy is to maintain constant incidence angle with respect to the surface; this facilitates comparisons of images from different areas. For more detailed information on the principles of SAR imaging and interpretation, see, e.g. Elachi (1987, 1988) and Johnson (1991).

The total width of the RADAR swath is created by combining the five individually illuminated sub-swaths (see Section 5.4) and ranges from 120 to 450 km at the spacecraft altitude, h, of 1,000 to 4,000 km. Each 1,000 km flyby of the RADAR Q8 will yield a SAR strip about 5,000 km long. Each such strip will image about 1.1% of Titan's surface. Over a tour in which, say, 25 close flybys would be available to the RADAR, at least 25% of Titan's surface could be imaged. This statement, although true in principle, needs to be qualified. As the example of the tours 18-5 and 19-1, introduced in Figure 3, illustrates, the SAR coverage is sensitive to the characteristics of a given tour—the segment of Titan repeatedly imaged in one tour may be invisible to the RADAR in another tour. Furthermore, the unavoidable overlap dictated by orbital dynamics reduces the aggregate SAR coverage in each tour.

3.2. ALTIMETRY

The altimetry mode will typically employ only the central, narrow antenna beam, to make time-of-flight measurements of the relative surface elevations along suborbital

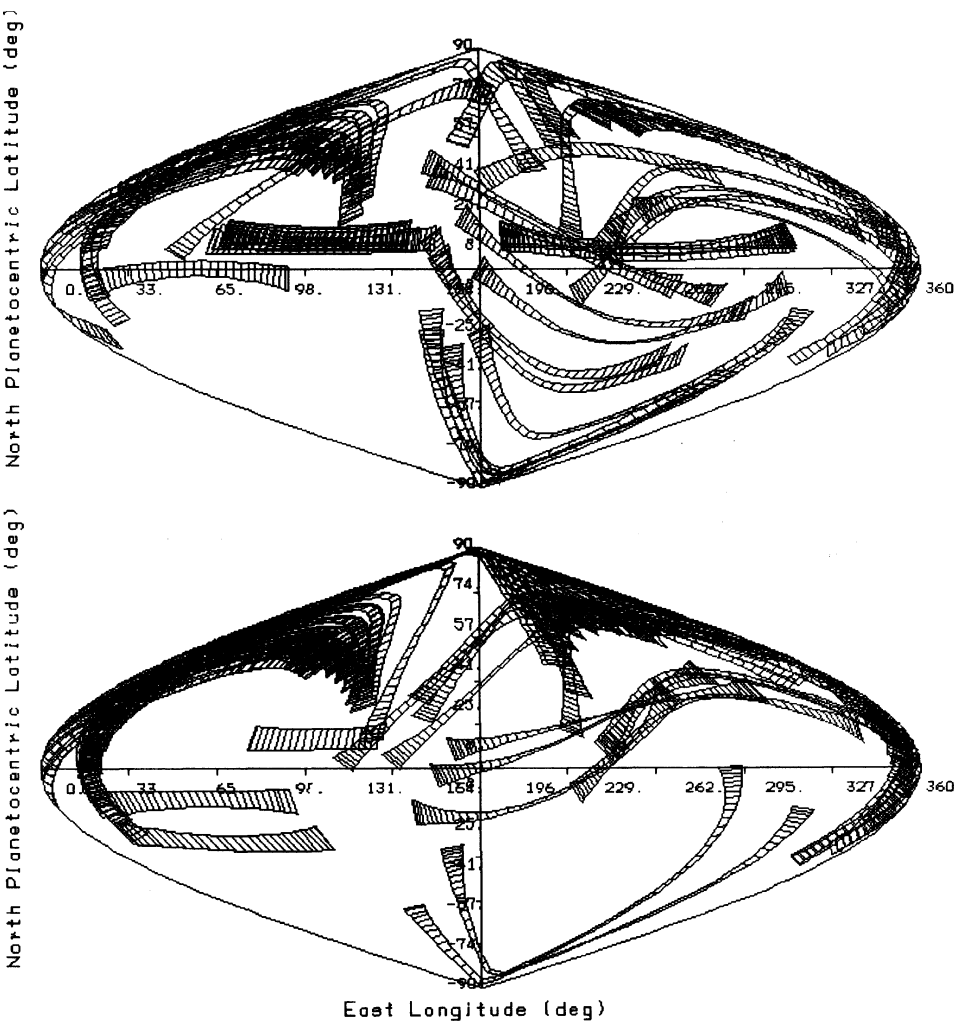

Figure 3. Mapping of Titan in the RADAR high- and low-resolution imaging modes. Included are only flybys with the close-approach altitudes <4,000 km; incidence angle 20°. (*Top*): Tour 18-5, (*Bottom*): Tour 19-1.

(nadir) tracks. Tight spacecraft pointing toward Titan's center of mass is required during the time altimetric observations are in progress. The primary information from the altimetry echoes is the range from spacecraft to surface which, taken together with the knowledge of the spacecraft and Titan ephemerides, will be converted into Titan's radii along the subradar track. Relative topographic accuracy will approach 150 m (see Section 4.1.2); absolute accuracy of radii will depend on the postflight ephemeris reconstruction accuracy, which has not yet been evaluated. Since complete return echoes are relayed to Earth, it is also possible to apply

appropriate scattering models to infer surface microtopography and reflecting properties, as has been done with the Magellan altimetry data (Ford and Pettengill, 1992; Tyler *et al*., 1992). The full length of a suborbital track for the spacecraft moving from the altitude of 10,000 km, through closest approach at 1,000 km, back to 10,000 km, is about 6,500 km. That is the maximum length of a topographic profile that can be obtained, assuming imaging is sacrificed to altimetry. For comparison, the currently available Goldstone altimetry profiles of Mars span no more than about 6,000 km (Downs *et al*., 1975). During a nominal Titan flyby (Figure 2), the two topographic profiles collected at the tail ends of imaging runs will each span about 750 km.

3.3. SCATTEROMETRY

The RADAR scatterometer mode measures the surface backscatter coefficient, σ_0 (radar cross-section normalized to the illuminated surface area), as a function of the incidence angle. From the instrument standpoint, this mode does not differ from the altimetry mode except for the reduced resolution; it has in fact often been referred to as "low-resolution altimetry." Since echoes at multiple incidence angles are desired, the spacecraft is commanded to scan preselected portions of Titan's disk between the nadir and limb, as during the RADAR radiometer observations. This mode allows radar echoes to be obtained from anywhere on Titan at a variety of incidence angles, albeit at resolutions much coarser than in the other active modes. An alternate mode manner of scatterometer operations, in which the RADAR central beam illuminates the icy satellites from a considerable distance, has been briefly outlined in Section 2.2.

3.4. RADIOMETRY

To acquire the RADAR radiometry data, three types of scans will be executed. Each will trace a spiral track on the surface of the target body. In two of these scans, only the central RADAR beam will be utilized; the third scan may involve one, three, or five beams. The first of the two central-beam scans is defined by a constant cone angle φ. The constant cone-angle scan yields data with a footprint of continuously varying sizes (Figure 4 (top)). In the second central-beam scan, the spacecraft is maneuvered so that the High Gain Antenna (HGA) describes an outward spiral and the boresight sweeps through a cone of increasing angular radius. Using parameters for the maneuvers appropriate to the approach velocity results in a nearly constant-resolution scan, balancing the decreasing range to Titan with increasing cone angle (Figure 4 (bottom)). Almost global coverage of Titan, at a resolution of about 500 km, is possible in a few judiciously selected flybys. Global coverage with a higher resolution will require scanning of Titan during each RADAR flyby.

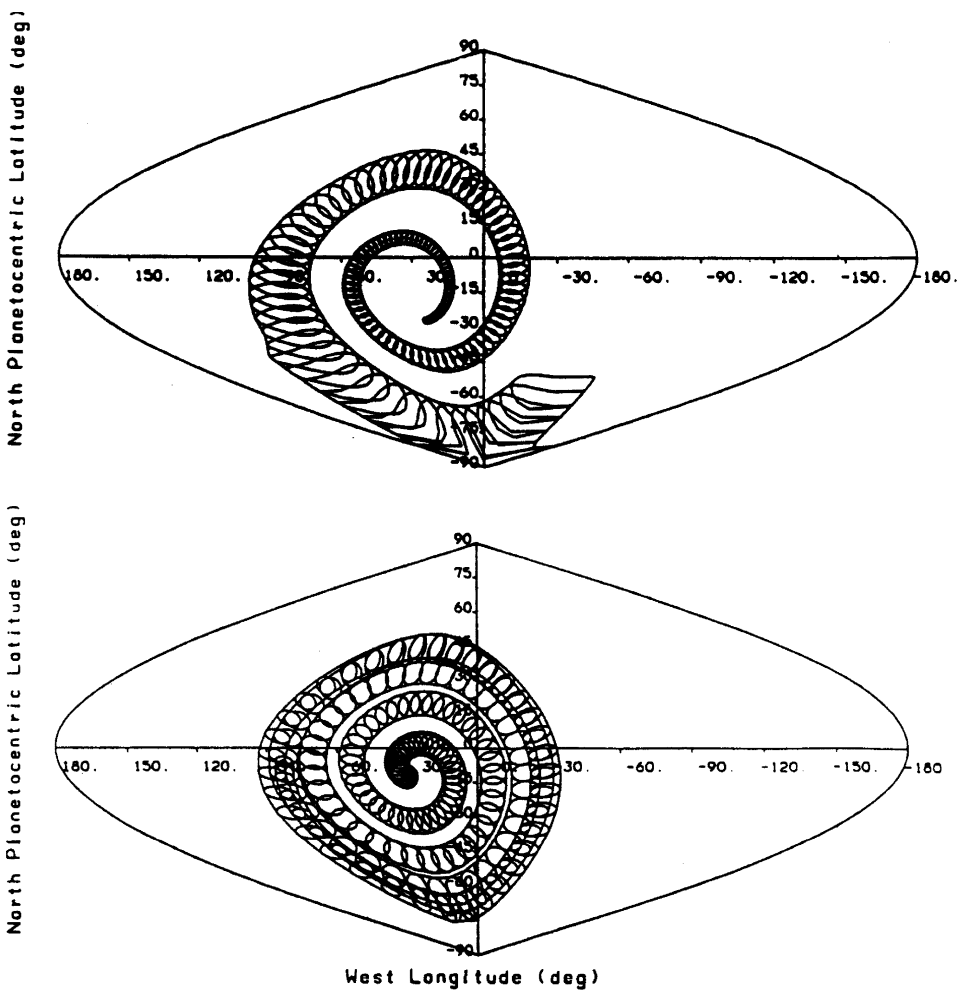

Figure 4. Scanning of Titan with the RADAR central beam. (*Top*): Constant cone angle; distance 100,000 km–10,000 km, clock rate 0.05° s^{-1}. (*Bottom*): Variable cone angle; distance 80,000–25,000 km, clock rate 0.20° s^{-1}.

When only the central beam aligned with the $(-z)$-axis is used during a scan, the spiral can be followed using small cyclic rotations about the x- and y-axis. The HGA nods in a circular motion, tracing out the spiral, but there is no cumulative rotation about the antenna boresight. In the third type of RADAR scan, when several beams are brought into play, the plane of the beam must be held perpendicular to the motion of the track. Consequently, as the spiral is followed, an additional rotation about the z-axis is also necessary. The rate and acceleration limits governing spacecraft under Reaction Control System (RCS) control (Table 8.8 in the Cassini Mission Plan, PD 699-100) place bounds on how rapidly the clock angle of the spiral in

either of the three scans can change. If ω is the clock rate, then $\omega\varphi$ must be less than $0.4^\circ\ s^{-1}$ and $\omega^2\varphi$ must less than $0.01^\circ\ s^{-2}$, at all times. Either of the three RADAR scans can be commanded by representing the surface track relative to the center of the target body as a sequence of vector polynomial segments in the Attitude and Articulation Control Subsystem (AACS) inertial vector table. An additional constraint that is imposed by the maximum frequency content of vector representations in AACS limits ω to less than $3.6^\circ\ s^{-1}$. Radiometry data will also be acquired during each of the active modes through the same beam used in the active mode (i.e. when transmitting) for that radar burst. The data will be acquired between the bursts.

3.5. Data acquisition scenarios

The RADAR will conduct its observations in the mission's RADAR/INMS operational mode. Because of similar requirements on Titan flyby geometry, the RADAR and the Ion and Neutral Mass Spectrometer (INMS) have been combined into a single mission operational mode; for the definitions of the mission operational modes, see Tables 8.1 and 8.4 in PD 699-100. Use of the RADAR modes depends primarily on (1) pass assignment; (2) flyby altitude; (3) science objectives; and (4) agreed-upon priorities among the instruments within the RADAR/INMS mode. Sharing Titan passes with other investigations may allow optimizing Titan observations for all parties, although these opportunities depend on, for example, the spacecraft being able to turn and change operational modes rapidly enough that the cost in overhead is small compared with the incremental science gain. The final observation strategy will be determined before arrival at Saturn; combined scenarios may indeed turn out to be attractive in their ability to maximize the amount of science data collected.

Ideally, the RADAR's full capabilities would be realized in a RADAR-dedicated Titan pass with a flyby altitude of 1,000 km or lower (Figure 2). In the interval between -6 and -5 h relative to the closest approach to Titan, and after the RADAR receiver had sufficiently warmed up, external radiometric calibration is performed by pointing the HGA at one or more predetermined calibration targets (cold sky, the Sun, the disk of Saturn, or a galactic radio source) and gathering thermal energy emitted by those targets. About 6 h before the closest approach, radar sequences are loaded. The subsequent operations are autonomous although coordinated with spacecraft maneuvers. At about -5 h ($h = 100,000$ km), the instrument commences observations in the radiometer mode as the spacecraft creates a scan pattern. Reception of thermal emission continues even when the RADAR is in active modes, but scanning using the spacecraft becomes less useful as the angular movement relative to Titan increases. At about -78 min ($h = 25,000$ km), the instrument begins active scatterometric observations. Depending on available maneuver time and desired targeting, either single- or multiple-beam observations

may be pursued. At about -30 min ($h = 9,000$ km), the spacecraft maneuvers to point the HGA in the direction of the Titan's center of mass. After this maneuver has been accomplished, altimetry begins. At about -16 min ($h = 4,000$ km), altimetry ends, the HGA is pointed 10–20° to one side of the ground track, and the low-resolution SAR imaging begins as the spacecraft executes the planned look-angle profile. At about -6 min, the spacecraft drops below an altitude of 1,600 km and the acquisition of high-resolution SAR images begins. This mode of operation will continue through the closest approach of Titan at altitude of 1,000 km. As the spacecraft recedes, the same sequence of the RADAR modes is executed in reverse.

While a few of the actual flybys of Titan may follow the standard sequence described above, there are at least three reasons for other, non-standard sequences. First, orbital dynamics is the driving factor for designing close Titan approaches into the tour and setting the dynamically optimal flyby altitudes. Thus, a number of flybys may occur at altitudes higher than 4,000 km, making SAR data acquisition unfeasible. Second, once the general physiography of Titan is known it may be more scientifically profitable to collect data in the other RADAR modes, over a particular target area. This may disrupt the standard sequence. Third, the needs of other instruments or an urgent spacecraft activity may interfere. For instance, in the vicinity of Titan, the principal non-science activity will be spacecraft tracking, which requires the HGA be pointed at Earth. As a result, the RADAR sequence may have to be truncated. In many cases, therefore, parts of the standard sequence may be mixed with other activities.

4. Radar Operations

The anticipated uncertainties in the spacecraft ephemeris and attitude predictions have led to a "burst timing" design for signal transmission and reception. In this timing approach, as shown in the lower portion of Figure 5, the radar transmits a series of pulses for a given time period and is then switched to receive the return echo burst. After reception, the radar switches to the radiometer mode to collect the surface-radiation measurements. With such an approach, the uncertainty in timing due to ephemeris and pointing errors will be accommodated by adjusting the burst period and data window rather than the pulse-to-pulse timing as in the case of the conventional pulse interleave approach. The chosen approach is expected to be more effective in utilizing the allocated data rate/volume, as well as in lowering the probability of data loss. The upper portion of Figure 5 illustrates the sequence of bursts as each antenna beam is used. For each beam the bursts overlap to give the multiple looks necessary in SAR in order that the speckle noise be reduced. A flyby with a closest approach altitude is used as an example in the following discussion but during actual operations the predicted profile will be used to set all the RADAR parameters for each pass.

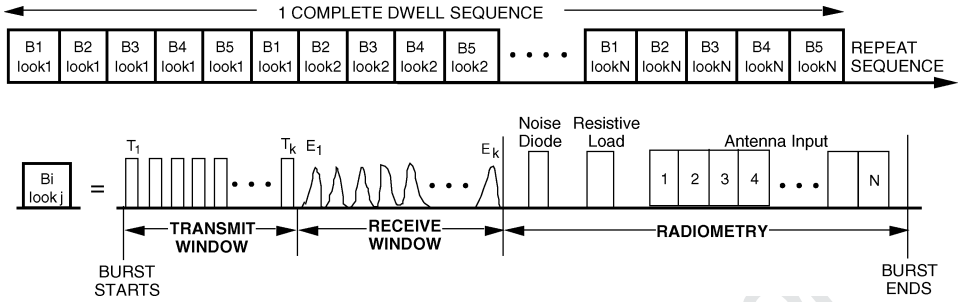

Figure 5. Non-interleaved multi-beam pulse burst timing for radar and radiometer operations.

4.1. RADAR MODES DESIGN

The motivation for the RADAR modes design is the desire to accommodate the potentially different types of surfaces on Titan (or other targets). Given the uncertainties in the ephemeris and in Titan's radar properties, the RADAR system performance must be robust. Since the radar range will be constantly varying within a single flyby as well as from flyby to flyby, the radar parameters such as pulse width, bandwidth, receiver gain, pulse repetition frequency, and other timing must be updated at regular intervals in order to maintain sufficient signal-to-noise ratio on the radar echoes. The major system parameters for each of the four instrument modes are listed in Table II.

4.1.1. *Imaging mode*

During radar imaging, the spacecraft will roll to either the left- or right-side of the suborbital track according to the pre-determined sequence, and five antenna beams will be utilized, one at a time, to obtain the maximum possible cross-track swath coverage (Figure 6). The azimuth image resolution will be accomplished by unfocussed SAR processing of the echo bursts. With the designed burst timing and processing schemes, the azimuth resolution, d_{az}, can be expressed as

$$d_{\mathrm{az}} = \frac{\lambda R}{2L_{\mathrm{SAR}}} = \frac{\lambda R}{2}\frac{1}{T_{\mathrm{B}}}\frac{1}{v_{\mathrm{sc}}\sin\theta} = \frac{\lambda R}{2}\frac{c}{2R}\frac{1}{v_{\mathrm{sc}}\sin\theta} = \frac{\lambda c}{4v_{\mathrm{sc}}\sin\theta}$$

where λ is the radar wavelength, R the range, L_{SAR} the unfocussed SAR aperture, T_{B} the echo burst period, c the pulse propagation speed, v_{sc} the spacecraft velocity, θ is the radar azimuth pitch angle, and $v_{\mathrm{sc}}\sin\theta$ is the spacecraft velocity component perpendicular to the radar line of sight (Im *et al.*, 1993). The azimuth resolution is estimated to be between 350 and 720 m throughout the imaging period of each flyby.

TABLE II
System Parameters for the Cassini RADAR Modes

	Frequency (GHz)	Peak power (W)	No. of beams	Look angle (°)		PRF (kHz)	Pulse width (ms)	Bandwidth (MHz)
				Cross-track	Along-track			
Imaging	13.78	46.2	All 5	5–20	0	1.8–6.0	200–400	0.43, 0.85
Altimeter	13.78	46.2	Beam 3	0	0	4.7–5.6	150	4.25
Scatterometer	13.78	46.2	Beam 3	±6 to ±12	±6 to ±12	1.0–3.0	500	0.11
Radiometer	13.78	N/A	All 5	±6 to ±12	±6 to ±12	N/A	N/A	135

N/A: Not available.

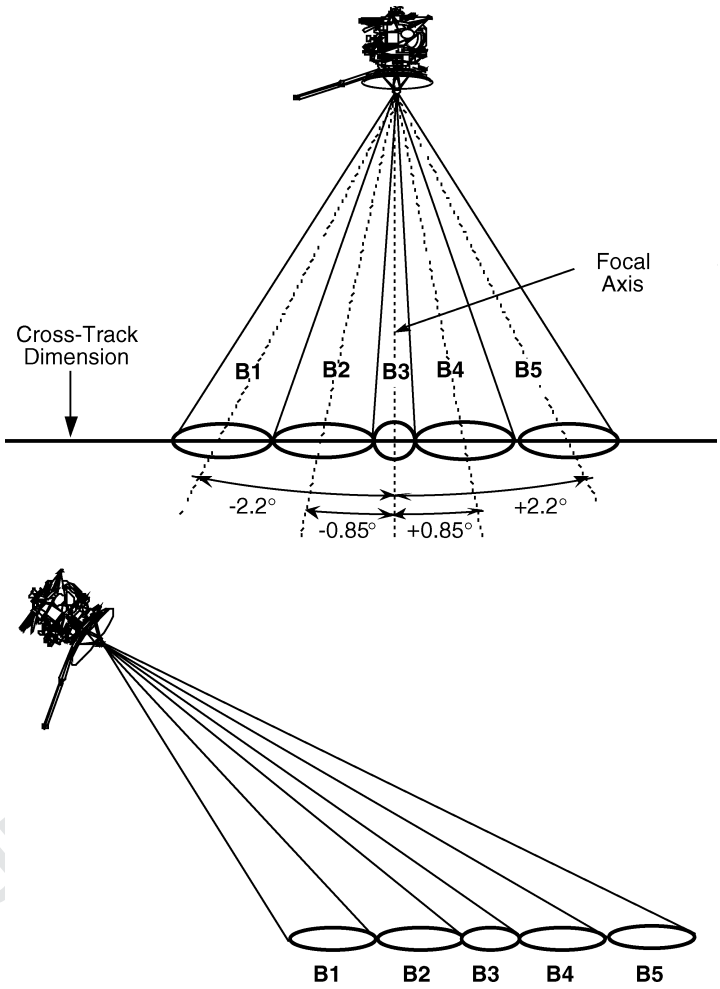

Figure 6. Antenna beam configuration for the Cassini RADAR. (*Top*): Nadir pointing for altimetry. (*Bottom*): Side-pointing for imaging.

The range resolution, d_r, is accomplished through range compression of the chirp signals:

$$d_r = \frac{c}{2B \sin \phi}$$

where B is the chirp bandwidth and ϕ is the incidence angle. In order to enhance the signal-to-noise ratio, a 850 kHz bandwidth will be used when the spacecraft altitude is 1600 km or less, and a 425 kHz bandwidth will be used at spacecraft altitudes between 1,600 and 4,000 km. The corresponding d_r is estimated to be between 420 m and 640 m at $h < 1{,}600$ km, and between 420 and 2,700 m at $1{,}600 \text{ km} < h < 4{,}000$ km.

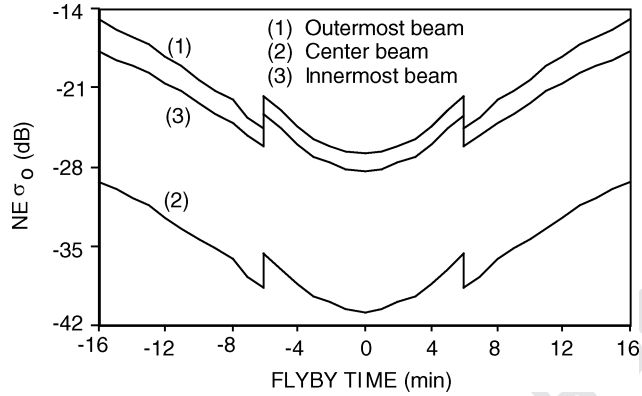

Figure 7. The σ_0 noise equivalent (NEσ_0) of the RADAR images during a nominal Titan flyby, with $h = 4{,}000$ km at $t = \pm 16$ min.

Due to the imperfect knowledge of the surface backscatter characteristics of Titan, we choose to use the so-called noise-equivalent backscattering coefficient, NE σ_0, as a measure of the signal detection sensitivity. This quantity is defined as the normalized surface cross-section which gives rise to a unity single-look thermal signal-to-noise ratio. That is,

$$NE\sigma_0 = \frac{2(4\pi)^3 kTBR^3 l_{\text{atm}}^2 \sin\phi}{P_T G^2 \lambda^2 r_{\text{a}} ct}$$

where k is the Boltzmann's constant, T the system noise temperature, l_{atm}^2 the round-trip atmospheric loss, P_T the radiated peak power, G the antenna gain, r_{a} the 3 dB along-track beamwidth, and t the pulse duration. Figure 7 shows NEσ_0 as a function of the flyby time for a typical Titan flyby with spacecraft altitude at the closest approach, h_0, equals 1,000 km. Due to the continuous change in both the range and Doppler contours as well as the irregular isogain contour of the offset antenna beams, the image ambiguity varies substantially throughout a Titan flyby. The total signal-to-ambiguity ratio is estimated to be $\geq$15 dB for all images obtained by the Cassini RADAR (Hensley and Im, 1993).

4.1.2. *Altimeter mode*

This mode will be used to generate relative elevations profile along the Cassini spacecraft sub-orbital track. Operating at spacecraft altitudes between 4,000 km and 9,000 km, this mode will utilize the nadir-pointing central antenna beam (Beam 3) for transmission and reception of chirp pulse signals at a system bandwidth of 4.25 MHz. The altimetric measurements along the sub-nadir ground track are expected to have horizontal resolution (pulse-limited radar footprints) ranging between 24 and 27 km and vertical resolution of about 50 m. The relative height change, Δh, over a surface region illuminated by two successive radar footprints

can be expressed as

$$\Delta h = (h_2 - h_1) - \frac{c(t_2 - t_1)}{2}$$

where h_2 and h_1 are the radar altitudes, deduced from spacecraft trajectory, at two points of interest and t_2 and t_1 are the corresponding round-trip flight times of the radar pulses. Since the trajectory perturbation is likely to be small, $(h_2 - h_1)$, and therefore Δh, can be deduced quite accurately during ground processing. We expect that an overall accuracy of 150 m can be achieved.

4.1.3. *Scatterometer mode*

The lack of reliable information on the backscattering characteristics of Titan's surface has been of major concern in the course of the RADAR design work. In order to compensate for the possibility that parts of Titan's surface are unexpectedly radar-dark, and to ensure credible measurements of the surface backscatter variations, we have incorporated a dedicated scatterometer mode into the overall design. The functional concept of the scatterometer mode is similar to that of the altimeter except for one major difference—the scatterometer bandwidth is but 106 kHz, to give sufficient signal-to-noise ratio at long ranges. The RADAR will operate in the scatterometer mode at altitudes between 9,000 km and 25,000 km. The spacecraft will be required to execute specified scanning maneuvers (spiral or circular). Both the backscatter and noise-only measurements will be collected, so that the surface backscatter coefficient, σ_0, can be estimated. Depending on the range distance and angle of incidence, this mode will detect σ_0 as low as -35 dB. The long-distance scatterometer observations of icy satellites, whose objective is to measure the disk-integrated radar albedoes, may also require execution of limited conical scans.

4.1.4. *Radiometer mode*

While operating in the radiometry mode, at a bandwidth of 135 MHz, the RADAR will measure the 13.8 GHz emissivity of Titan and targets of opportunity. The radiometer mode can be used alone or in conjunction with other RADAR modes. The data are collected as shown in Figure 7. During each burst, after the active portion of the radar cycle is completed, the radiometer first switches to the noise diode as input, and then to the resistive load in the Front End Electronics (FEE). Each of these calibration sources are sampled once per burst, and the integration times are set to yield between 2,000 and 3,500 counts in a 12-bit (4095) counter. After the two calibration measurements are made, multiple measurements (up to 255) are made through the antenna port. These multiple 12-bit values are summed to give one 20-bit value per burst. Thus, during each burst three radiometer data-points are recorded. Before and after each radiometer only data-taking the HGA will be turned to "cold-space" for an absolute calibration of the antenna-input relative to the internal calibration sources. According to our estimates, the RADAR radiometer is capable of measuring brightness temperature with an error of less than 3 K.

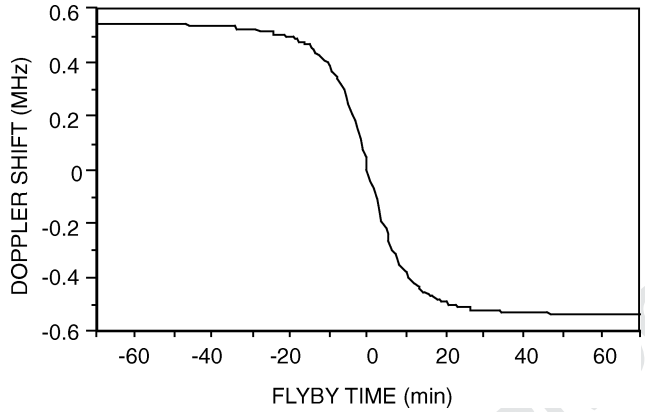

Figure 8. The Doppler shift during a nominal Titan flyby, with $h = 22{,}500$ km at $t = \pm 70$ min.

4.2. DOPPLER TRACKING

Due to the spacecraft motion, the received radar signal will be Doppler-shifted. The extent of the shift depends on the antenna pointing, frequency, and orbit geometry. Assuming that the antenna is pointed toward the center of Titan at any time during a flyby, the maximum Doppler shift, Δf, will be less than ± 600 kHz, for a flyby altitude of 1,000 km at closest approach. The Doppler shift profile versus flyby time is plotted in Figure 8. In our current design, the chirp signals will be generated digitally with center frequency shifted by an amount equal to $-\Delta f$ in order to compensate for the shift. Other factors such as the trajectory perturbations, finite-time updates, and off-nadir antenna pointing will also contribute to the shift. The receiver filters compensate for these shift residues.

4.3. ONBOARD DATA REDUCTION

Signals to be acquired by the active radar modes will initially be quantized to 8 bits. In order to satisfy the allocated output data rate constraint, the radar data will be re-quantized onboard to a lesser number of bits, using the block-adaptive quantization (BAQ) scheme similar to the one used by the Magellan radar. In this scheme, the 8-bit digital samples per interpulse period are divided into a finite number of blocks. After signal averaging over a number of pulse periods, the averaged power in each block is estimated and a threshold is determined. The 8-bit data are then scaled with respect to the threshold and the scaling factor is quantized to k bits ($k < 8$). Both the scaling factor and the threshold values, after quantization, will be downlinked for signal reconstruction purpose. This, together with the lesser number of bits used for the scaling factors, reduces the output data rate substantially. Our current estimates of the output data rates are: 195 and 250 kbps in the imaging mode, low and high resolution, respectively, (8-to-2 reduction), 30 kbps in the altimeter and

scatterometer modes (8-to-4 reduction). We use a larger number of bits for altimetry and scatterometry due to the fact that in these modes less data are averaged and the initial data rates are lower.

4.4. Control instructions

The timing, gain, antenna port selection, and other setup parameters of the RADAR are controlled through a set of instructions which are calculated on the ground and uplinked to the spacecraft prior to a flyby. After the RADAR is turned on and the FSW loaded and started, the Instruction Execution Block (IEB) is loaded and triggered. The block contains all the instructions the FSW will execute during a flyby. There are three types of instructions: Power—to control the power states of the RADAR; Telemetry & Command—to set up special modes, including diagnostic instructions; and Slow and Fast instructions. The last two are combined into one setup instruction for the RADAR configuration. The reason for the fast and slow types was to reduce the number of instructions necessary to uplink by recognizing that some parameters vary faster than others.

Tables III and IV present a list of the slow and fast instructions and their meaning. A much more detailed description of each parameter is in the Cassini RADAR Digital Subsystem High Level Design Document (DSS-HLD). During a typical flyby it is expected that each Fast Field will change as often as every 15 s while each Slow Field will change as often as every 3 min. The execution time for each instruction is controlled by the flight software, using the relative time from the initial trigger (TFI) of the RADAR. The combined instruction is sent to the Control and Timing Unit (CTU) for its actual control of the RADAR. The TRIGGER command is the last command the RADAR, received from the spacecraft Command and Data System (CDS) prior to RADAR operations and from that point on, until the RADAR is turned off, the RADAR operates autonomously.

4.5. Instrument data modes

The RADAR sends data to the spacecraft CDS for storage on the Solid State Recorder (SSR) through two channels. The first, low-rate (10–20 bps), channel is called "Housekeeping" and is used whenever the RADAR is on. The Housekeeping channel carries engineering data only. It becomes active approximately 80 s after the DSS is turned on and continues until the DSS is turned off. During normal operations a complete sample of RADAR engineering data is received every 2–4 min. The second channel is the High Rate Science channel with data rates as high as 365 kbps. All RADAR science data, including the engineering data in the science headers, are sent through this channel. The spacecraft CDS picks up packets from the RADAR at the maximum rate of 365 kbps but only stores

TABLE III
Slow Field Instruction Structure

Parameter Name	Bits	Range
Time from trigger	16	0–18.2 h in 1.0 s steps
Instruction type	2	11_2 (fixed)
Data take number	8	0–255
Slow field instruction number	8	0–255
Radar mode	4	0: LALTL, 1: LALTH, 2: SARL, . . .
Calibration source	4	0: Norm, 1: Ant, 2: Noise diode, . . .
Adc sample rate	2	0: 0.25, 1: 1.0, 2: 2.0, 3: 10.0 MHz
Receiver bandwidth	2	0: 0.12, 1: 0.47, 2: 0.94, 3: 4.68 MHz
Transmit/receive window offset	4	-8 to $+7$ PRIs
Data compression mode	3	0: 8/2, 1: 8/1, 2: 8/1MSB, . . .
Beam mask	5	00100_2: beam 3, 11111_2: all beams
Receiver attenuattion (beams 1 and 2)	12	0–74 dB in 1 dB steps
Receiver attenuattion (beam 3)	12	0–74 dB in 1 dB steps
Receiver attenuattion (beams 4 and 5)	12	0–74 dB in 1 dB steps
Radiometer integration period length	4	10–75 ms in 5 ms steps
Number of radiometer integration periods	8	1–255 periods
Chirp step duration	8	0.67–9.47 μs in 0.67 μs steps
Chirp step quantity	12	2–750 steps
Chirp frequency step size	16	0–117.2 kHz in 1.788 Hz steps

TABLE IV
Fast Field Instruction Structure

Parameter Name	Bits	Range
Time from trigger	16	0–18.2 h in 1.0 s steps
Instruction type	2	10_2 (fixed)
Fast field instruction number	8	0–255
Bursts in instruction	8	1–255 bursts
Pulses in transmit burst	8	0–255 pulses
Burst period	12	10–4095 ms
Receiver window delay	10	0–1023 PRIs
Pulse repetition interval	10	0–1023 clock periods
Chirp start frequency	16	0–30 MHz (458 Hz steps)

those packets that have real data included. The other packets are identified as "0-filled" by the RADAR and are discarded. The valid data are produced by the RADAR at variable rates; typically 1 kbps for radiometer only, 30 kbps for scatterometer and altimeter, and up to 260 kbps for imaging. It is up to the RADAR to insure that the total volume of data allocated to the RADAR is not exceeded during the RADAR data collection time. The total volume of data the RADAR would produce in the course of a nominal Titan flyby (i.e. a 1,000 km flyby) is about 1 GB.

During the cruise period, when only a simple preventive maintenance test is performed every three months, the only data-type available is housekeeping. Normal operations of the RADAR will be executed during infrequent special checkout periods.

4.6. MAINTENANCE SEQUENCE

The maintenance sequence the RADAR will execute every three months during the cruise phase of the mission is shown in Figure 9. The figure illustrates how the CDS and the RADAR interact during this sequence, and is also illustrative of how the RADAR will be operated during science data taking. The thick center line represents

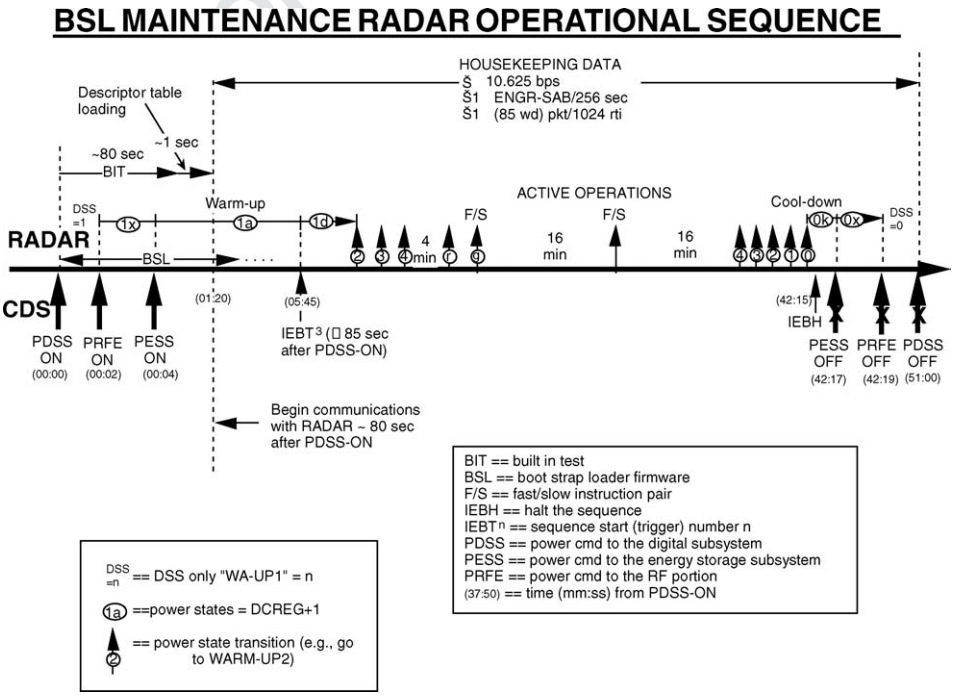

Figure 9. The RADAR Bootstrap Loader Maintenance Sequence.

a timeline interface between the RADAR and the CDS; the CDS actions are below the line, the RADAR actions above. The times after the DSS turn-on are shown with each command from the CDS. The three RADAR power switches are quickly turned on to start the RADAR. The RADAR DSS goes through an initialization procedure during which a sequence of built-in tests is run. After these tests are completed the RADAR loads a descriptor table into the CDS/RADAR interface, and communication with the RADAR can begin. It is at this point that the housekeeping data start to be sent to the CDS. As the maintenance sequence runs from PROM (the Bootstrap Loader), no flight software or an IEB table are necessary to be loaded prior to operations.

The RADAR comes up in a power state called Warmup-1. This power state has several substates, depending on which commands have been sent by the CDS. As soon as the RADAR receives a trigger, the PROM sequence of instructions begins to run. These are illustrated by the short up-arrows above the time line. The numbers embedded in these arrows indicate a transition instruction to that power state. These power states are for the RFES portion of the RADAR. The transition to the Warmup-4 includes a 4 min wait to allow for time to warm up the Traveling Wave Tube Amplifier (TWTA). The last power instruction puts the DSS in the state to sequence the RFES. The first fast/slow (F/S) instruction then commands the transmitter to commence transmitting.

In the maintenance sequence there are only two fast/slow field pairs which operate for 16 min each. The RADAR transmits and receives, but no science data are collected. After the end of the second 16 min period the power instructions reverse the order to put the RADAR in Warmup-0 mode, and make it ready for the power to be disconnected by the CDS commands to the power subsystem of the spacecraft. The housekeeping data transmission ends when the DSS is turned off but, in reality, the last housekeeping packet received represents the state of the RADAR several minutes before shutoff.

5. RADAR Design Considerations

The Cassini/Huygens mission is a joint undertaking of the National Aeronautics and Space Administration (NASA), European Space Agency (ESA), and the Italian Space Agency (ASI). The RADAR instrument was developed in partnership between NASA and ASI. ASI selected Alenia Aerospazio in Rome as the contractor for both the spacecraft High Gain Antenna (HGA) and the RADAR Radio Frequency Electronics Subsystem (RFES). Alenia in turn selected subcontractors such as FIAR in Milan and EMS in Atlanta, Georgia, for the component units of the RFES. The overall responsibility for the RADAR system design and spacecraft interfaces rested with the Jet Propulsion Laboratory (JPL). The complexity of the instrument called for a number of special design considerations. We treat here the following: power, mass, space and location, antenna, pointing and ephemeris

accuracies, target-flyby geometries, instrument control method, data rates and volumes, and the limited number of Titan flybys.

5.1. Power

The Cassini spacecraft power system uses radioactive thermal generators (RTGs) for all its electrical power and no batteries for power buffering. The RADAR has high (195 W) peak power requirements which could not be accommodated by the spacecraft power system. Early design of the instrument included an internal battery which would provide most of the transmitter energy requirements during a 10 h Titan flyby. Both battery size and long life considerations led to a battery substitute, called the Energy Storage Subsystem (ESS), which is a bank of capacitors. The design of the ESS called for energy to be stored for a "transmit burst," 90–3,000 ms. The transmit portion of the burst lasts no more than about 10% of the total burst time, thus, the 90% non-transmit time is used to recharge the capacitor bank of the ESS. The peak transmitter power requirement was thus reduced from 195 to 30 W by use of the ESS. The RADAR power requirement is 86 W.

5.2. Mass

As in all planetary missions, mass has been a severe constraint on the RADAR design. Conservative design for an 11-year mission and radiation environments near 100 krad dictated the use of low-density components. This resulted in the total mass of 43.3 kg for the RADAR instrument.

5.3. Space and location

The spacecraft was designed to have 12 electronic bays. The RADAR occupies Bay 11 and a specially constructed appendage to the main body of the spacecraft, the "penthouse" (Figure 10). The use of the penthouse required a thermal interface through a baseplate to the spacecraft; it further required additional thermal blankets, louvers, and radioactive heating units (RHUs) to control the thermal environment of the RFES. The DSS and ESS, located in Bay 11, share the thermal design of the spacecraft bays.

5.4. Antenna

Tight constraints on mass and volume required that the RADAR share the 4 m telecommunications antenna (HGA), as did the radar on the Magellan mission. The system design also dictated that a single feed or beam could not meet the per-flyby requirements of imaging and other modes simultaneously. A five-feed, five-beam design was decided upon, in which the center, highest-gain beam would be used in

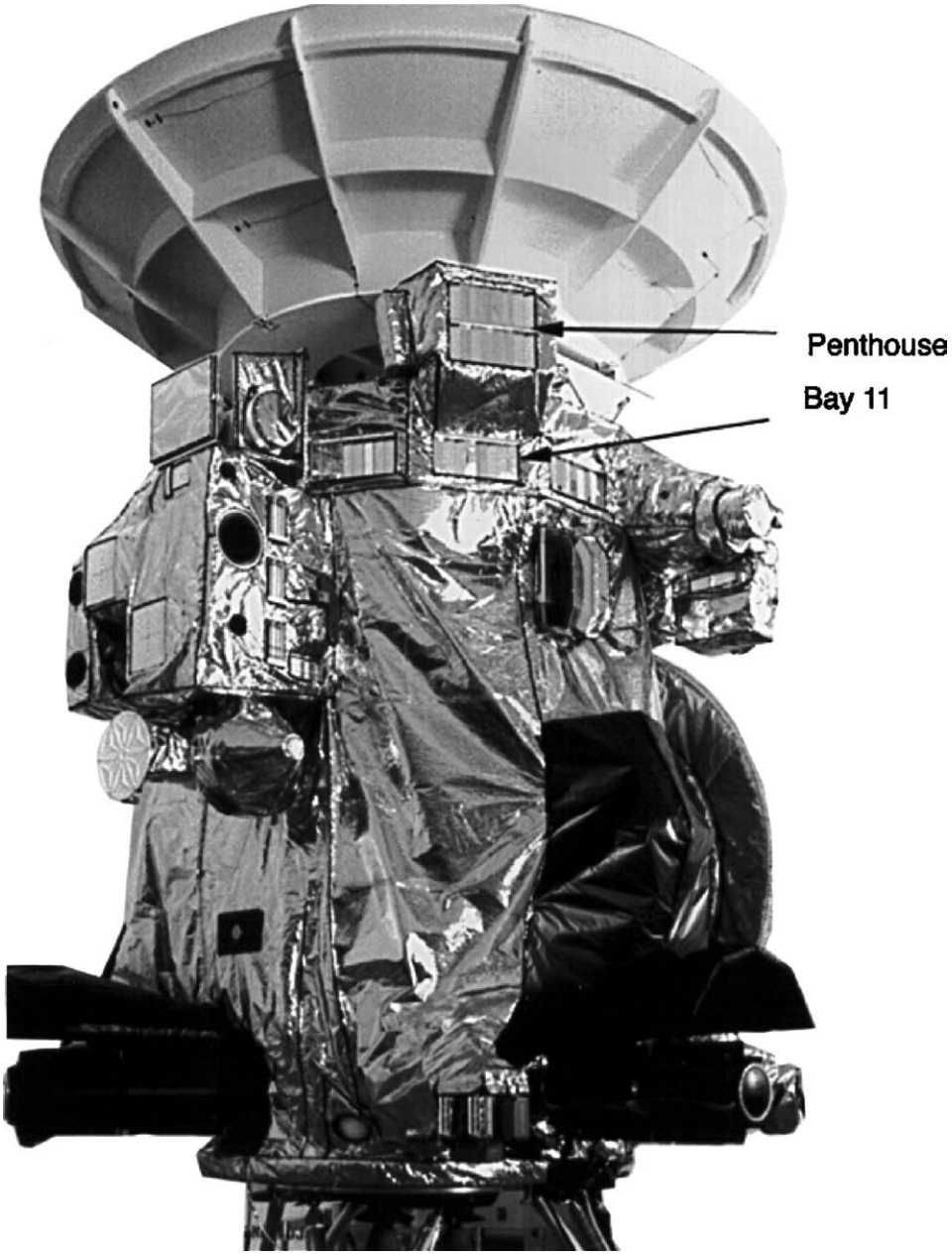

Figure 10. The locations on the spacecraft of the RADAR RFES (Penthouse) and DSS/ESS (Bay 11).

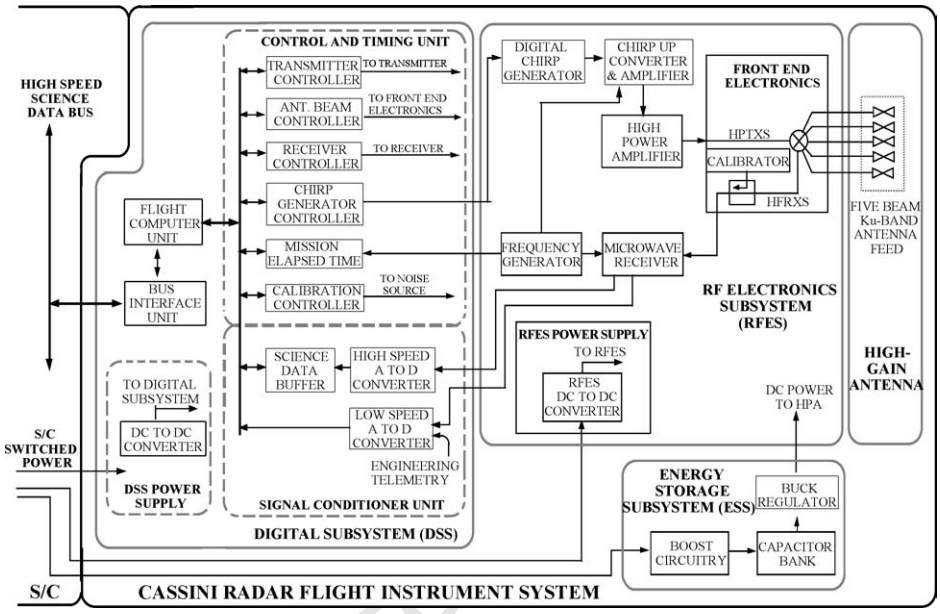

Figure 11. Cassini RADAR block diagram.

all modes. The additional four beams would be used in the imaging mode, creating a wide swath. Beam switching would be done inside the RADAR. The five-beam design required five waveguides into the HGA, each with a separate feed. Other methods of beam scanning were considered, such as the phased-array feeds, but were rejected. The five feeds were accommodated into the four-frequency HGA (Figure 11). The switching of the beams is accomplished in the RFES by the Front End Electronics, which is a compact set of twisted waveguides and circulators. No moving parts were used.

5.5. Pointing and Ephemeris

In order to automatically record the echo data the RADAR needs to have available accurately predicted ranges to the targets of interest. This is achieved by knowing at any instant the spacecraft position relative to the target and the HGA pointing. Since the Cassini spacecraft is in orbit around Saturn, and Titan is the target of interest, the accuracy of the ephemeris is expected to be insufficient by Earth-observing or Magellan radar standards. The same is true for pointing, which is done relative to a star field or a fuzzy limb rather than the center of Titan, and is thus degraded for radar use. These inaccuracies demanded a design in which the radar echoes are not interleaved with transmissions, as would be required for high-resolution imaging. Thus, the radar transmits for a set number of pulses and pulse rate until

the prediction indicates the first echo will have returned, and then the receiver is activated and all echoes received.

5.6. Flyby geometry

As described in Section 4.6, the timing of the radar must be set properly to receive the echo. It is also necessary that the frequency of the echo be within the range of the receiver. If the target is moving with respect to the transmitter or the receiver, the echo is Doppler-frequency shifted proportional to the velocity and radar frequency. Normally this shift is only a small fraction of the bandwidth and can be neglected. For the Cassini RADAR, the bandwidth is as low as 0.1 MHz and the Doppler shift as high as ± 0.6 MHz. It is a requirement on the design to take into account this effect.

5.7. Control method

The control of the radar can be performed by several means including remotely, based upon predictions, and automatically, based upon actual data. The radar echoes and radiometric settings, it was felt, would be too difficult for an automatic system to set up and hold to all the system constraints, especially that of the total data volume. A computer was available on the project list, called the Engineering Flight Computer (EFC), which had most of the capability required for radar operations. It was decided that the radar parameters would be table-driven from a time-ordered set of parameters, which would control all the radar parameters such as gain, antenna port, pulsewidth, and bandwidth. Each entry in the table is calculated by ground software, called the Radar Mapping Sequencing Software (RMSS), which takes inputs such as science desires spacecraft pointing, ephemeris, and data rate. The RMSS outputs the Instruction Execution Block (IEB) table. Each RADAR observation (a Titan flyby, an icy-satellite flyby, etc.) has a unique table which is transmitted to the spacecraft as part of the regular uplink process prior to a flyby.

Another aspect of RADAR control is the program, which runs in EFC. This program is called the Cassini RADAR Operational Control Flight Software (CROCFSW), or Flight Software (FSW) for short. The FSW, to be described later in this paper, is a major contributor to the functionality and testability of the RADAR hardware.

5.8. Data rates and volumes

In addition to mass and power, the data rates and volumes are the most limiting resources planetary missions impose. During each RADAR flyby of Titan about 1 Gbit will be recorded on the spacecraft's Solid State Recorder (SSR) for later playback. These data include all spacecraft packet formats, radar formats, engineering

telemetry, and science data. The science portion will be approximately 90% of the total. In order to pack as much information as possible into these bits the echo data are compressed using a method pioneered on the Magellan mission called the Block Adaptive Quantizer (BAQ) (Kwok and Johnson, 1989). On Magellan, the method used was 8-bits-in/2-bits-out (8/2), in a fixed hardware design. In the case of the Cassini RADAR the hardware method was dropped and a software method added to the system. Since the BAQ was implemented in software, it has much more flexibility than the Magellan hardware method; in fact, other modes are available such as 8/4, 8/1, and 8/0. The 8/4 mode will be used for altimetry and scatterometry, the 8/1 mode could be used for imaging in order to sacrifice amplitude resolution in return for finer spatial resolution, and the 8/0 mode (which produces no data) is used for test purposes.

5.9. Limited number of flybys

The RADAR lacks opportunity to acquire processable echoes prior to its first data-collecting flyby of Titan, likely to take place in 2005. Radar-operational flybys of Venus and Earth would allow the first closed-loop test of the RADAR system. As helpful as these tests could be, they would still simulate operations at targets vastly different from Titan. The review in Section 1 showed how little we know about the surface characteristics of Titan. We know even less about the performance of the RADAR radiometer and about the thermal effect of a 10 h RADAR flyby of Titan on the performance of the spacecraft systems. During the Science Cruise (i.e. in the period of 2 years prior to the Saturn Orbit Insertion), we expect to run extensive "dress rehearsal" tests to simulate full Titan flybys. During a Titan flyby the HGA is pointed at Titan, and no data are received at Earth. Thus, there is no opportunity to correct problems during the data collection, and if there indeed are problems, the RADAR flyby will, most likely, be sacrificed and the correction will have to wait until the next downlink/uplink cycle is completed. To make this process efficient, the RADAR has been designed to be as autonomous as possible and monitor and report all aspects of its operation while collecting the science data.

Prior to each flyby the RADAR is powered up, at which time it performs a series of built-in tests (BITs). The results of the BITs are reported in the low-rate housekeeping data. Next, the FSW is loaded, followed by the IEB table and by the trigger to start. If any of these processes does not go to completion the RADAR cannot report that fact to the spacecraft and the science-data flyby will be lost. If a problem occurs after the trigger, the FSW should recognize that fact and recovery might be possible, depending upon the nature of the problem.

In addition to potential hardware (or software) faults the data themselves can be examined by the FSW to determine if the settings of the radar system parameters are correct. The three areas which were examined for automatic control (onboard

processing) were the timing of the receive window position, receiver gain, and radiometer integration period. It was felt that it would be difficult to set the timing correctly in an automatic system in all cases and that the pointing and ephemeris would be good enough for data capture so automatic timing control was rejected. Receive gain control was examined and determined to be a candidate for automatic control. Consequently, automatic gain (really attenuation) was implemented as well as automatic radiometer integration-time setting. Each of these software modules reads the input science data and determines a change in the setting, which will bring the level closer to the ideal.

6. Hardware Design

The Cassini RADAR consists of four subsystems: the Digital Subsystem (DSS), Radio Frequency Electronics Subsystem (RFES), Energy Storage Subsystem (ESS), and High Gain Antenna (HGA) (Figure 11). The DSS, built at JPL, contains the interfaces to the spacecraft data bus, the control electronics for all the radar, the analog-to-digital converters for both science data and engineering telemetry, and the flight software for all RADAR operations. These operations include data assembly and data processing such as gain adjustment and data compression. The RFES, built by Alenia Aerospazio, contains all the analog RF components of the RADAR as well as the digital chirp generator (DCG) and the Ultra-Stable Oscillator (USO)—the timing reference for the whole RADAR. The RFES responds to digital signals from the DSS, to set its operating parameters. The ESS, built at JPL, is a battery substitute for the transmitter of the RFES. The HGA, built by Alenia Aerospazio, has four frequency bands (S, X, Ku, and Ka) to provide services for radar science (Ku-band) and radio science and telecommunications operations (the remaining bands).

6.1. Digital subsystem

The Digital Subsystem performs all the digital functions of the RADAR, which include accepting commands from the spacecraft Command and Data System (CDS), executing the flight software, operating the entire system as specified in the uplinked instruction table, collecting and processing science data, and collecting engineering telemetry data. The DSS is located in a portion of Bay 11, one of the 12 bays, which make up the spacecraft instrument bus. The DSS is made up of five circuit chassis which contain the following: the Flight Computer Unit (FCU), the Science Analog-to-Digital Converter (SADC), the Telemetry Analog-to-Digital Converter (TADC), the Science Data Buffer (SDB), the Control and Timing Unit (CTU), the Power Converter Unit (PCU), and the RFES interfaces. The functions of each of these units are explained below.

6.1.1. *Flight computer unit*

The Flight Computer Unit is made up of the project-supplied Engineering Flight Computer (EFC), the Bus Interface Unit (BIU), and Startup Read Only Memory (SUROM). The function of the FCU is to accept and interpret commands from the spacecraft CDS. The commands include the RADAR flight software and the table that contains the time-ordered set of instructions to operate the RADAR. The FCU controls both science and engineering telemetry data flow, compresses the science data using a software algorithm known as the Block Adaptive Quantizer (BAQ), and formats the data into RADAR units known as SAR-Altimeter Bursts (SAB) and then into the smaller CDS transport packets.

6.1.2. *Science analog-to-digital converter*

The Science Analog-to-Digital Converter (SADC) is known as the "Science ADC" to distinguish it from the ADCs for the telemetry subsystem and the radiometer. The Science ADC consists of three parts: an input buffer amplifier, the high-speed ADC, and the digital code conversion circuitry and output buffers. The input buffer amplifier receives the video signal from the receiver, amplifies it, and level-shifts it to a value that is compatible with input voltage range of the ADC. The digital circuitry receives and transmits all control and timing signals required by the Science ADC Subsystem.

6.1.3. *Telemetry analog-to-digital converter*

The purpose of the Telemetry ADC Subsystem (TADC) is to provide the Engineering Flight Computer (EFC) with up-to-the-second data on the performance of the Cassini RADAR System. The TADC samples analog voltages from DSS, ESS, RFES, and external waveguides, converting them into digitized equivalents with an analog-to-digital converter, and then it transfers those digitized data into RAM memory. The TADC also accepts the radiometer DC signals from the RFES and processes them for inclusion in the SAB footer.

6.1.4. *Science data buffer*

The Science Data Buffer (SDB) is a 16K-word, high-speed RAM buffer that acts as a rate buffer for science data from the high-speed A/D converter (SADC) enroute to the FCU. The SDB appears in the address space of the FCU as a 16K-word (one "word" equals two bytes) block. During the receive-window of a burst, the SDB is filled with raw, 8-bit, time-domain samples (packed two samples per word) from the SADC. When the receive-window closes, the FSW transfers the burst of data from the SDB into the local memory of the FCU.

6.1.5. *Control and timing unit*

The Control and Timing Unit (CTU) sets all the timing functions of the RADAR. It accepts a formatted instruction from the software running in the FCU and stores it in a register until the previous instruction runs out. The CTU sets all the high-speed

logic in the RADAR such as when to transmit, when to receive, or when to move data to the RFES. The CTU runs off a 10 MHz clock that is derived from the 30 MHz Ultra-Stable Oscillator (USO) in the RFES.

6.1.6. *Power converter unit*

The Power Converter Unit (PCU) takes the 30 VDC power from the spacecraft power bus and converts it to the various voltages used in the DSS: ±5 VDC, ±9 VDC, −12 VDC, and ±15 VDC. The power into the PCU comes from the spacecraft via a solid-state power switch, one of the three used to control the RADAR.

6.1.7. *RFES interfaces*

The electrical interfaces to the Radio Frequency Electronics Subsystem (RFES) are all with the DSS, except for the power interfaces to the spacecraft and to the RADAR Energy Storage Subsystem (ESS) and the RF interface with the HGA. There are 22 control and timing signals from the DSS-CTU which, among other things, control the beam-select and receive-window. In the RFES the signals fan out to the various units such as the Front End Electronics for beam-select and Microwave Receiver for receive-window. A high-speed logic line also controls the waveform generation start in the Digital Chirp Generator. The DSS accepts analog inputs from the RFES such as the downconverted waveform going to the SADC, and the radiometer and engineering telemetry voltages going to the TADC.

6.2. RADIO FREQUENCY ELECTRONICS SUBSYSTEM

The Radio Frequency Electronics Subsystem (RFES) is that portion of the RADAR that converts the chirp waveform data from the DSS into high-powered pulsed waveforms which, in turn, are sent to the proper antenna port. The echoes are received through the same port and captured by the sensitive receiver. The physical location of the RFES is in a "penthouse" located above Bay 11 (which houses the DSS), below the backside of the HGA (see Figure 10). The penthouse is attached thermally to the spacecraft through a baseplate and has additional thermal control through the use of thermal blankets, a louvered outer cover, and five 3 W, radioactive heating units (RHU) attached to the outer surface of the RFES. The units which make up the RFES are the Frequency Generator (FG) (which contains the Ultra-Stable Oscillator), the Digital Chirp Generator (DCG), the Chirp Upconverter and Amplifier (CUCA), the High-Power Amplifier (HPA), the Front End Electronics (FEE), the Microwave Receiver (MR), and the Power Converter. The operation of these units will be explained below.

6.2.1. *Frequency generator*

The Frequency Generator Unit (FGU) contains the 30-MHz USO that is placed in an oven controlled to 85 °C. The signals from this unit are sent to three destinations.

First, they are sent to the CUCA, to provide upconversion frequencies for construction of the transmit waveform. Second, they are sent to the MR, to downconvert the received signal to baseband. Third, they are sent to the DSS for all digital timing signals control, including the digitization of the science data.

6.2.2. *Digital chirp generator*

The Digital Chirp Generator (DCG) is the device that generates the frequency-modulated signal, the "chirp." The chirp is the pulse expansion necessary in high-performance radar in order to achieve high average power with relatively low peak power. The inputs to the DCG come from the DSS; they are the parameters of a pulsed radar chirp—such as the start frequency, number of frequency steps, frequency step length, and frequency step size. The last three parameters control the pulse length and bandwidth, while the first controls the frequency offset due to the high Doppler frequencies on this mission.

6.2.3. *Chirp upconverter and amplifier*

The chirp signal coming from the DCG is at baseband frequency and of low level. In order to drive the transmitter, the chirp waveform must be upconverted to 13.8 GHz and amplified. The Chirp Upconverter and Amplifier receive the low-level chirp from the DCG. It uses the 30 MHz signal and derivatives to arrive at 13.8 GHz, and then the signal is amplified to the proper level.

6.2.4. *High power amplifier*

The amplified chirped signal from the CUCA is further amplified by the High Powered Amplifier (HPA) to approximately 65 W peak power. The HPA uses a traveling wave tube amplifier (TWTA). This tube operates at high voltages (4,000 VDC) in order to get sufficient amplification. The high voltages are generated within this unit. The output of the HPA is fed through waveguides to reduce losses.

6.2.5. *Front end electronics*

The purpose of the FEE is to route the transmitted signal through one of the five output waveguides and to switch a few milliseconds later to route the echo to the receiver. The FEE is a complex set of 13 circulators and waveguides, which allow selection of single beams a large number of times without deterioration of function. The FEE also contains the resistive load calibration for the radiometer and the routing circuit for the injection of the noise diode calibration. The noise diode itself is located in the MR.

6.2.6. *Microwave receiver*

The most complex unit in the RFES is the Microwave Receiver. This unit contains the low-noise amplifiers (LNA), downconverter, amplifiers, bandpass and bandwidth filters, variable attenuators, and the radiometer detection circuit and noise diode calibration source. Because of its extreme sensitivity, a limiter was added

before the LNA to reduce the possibility of catastrophic failure caused by high signals entering the MR. The LNA were specially designed and mounted in gold foil to reduce gain changes that might result from the ground-plane motion. To protect the LNAs during normal operations, pin-diode switches block signals except when reception is desired. A combination of high-gain amplifiers and attenuators, controlled from the DSS, allow for precise control of the signal levels going to the DSS-SADC.

The radiometer detector circuit operates at the full 135 MHz bandwidth of the receiver. The circuit contains a special noise diode, an integrator, and a reset circuit. Particular consideration was given to all these components to yield a stable system. The noise diode has undergone special gold foil application for grounding to reduce gain jumps. The diode is mounted in a kovar frame, and its signal goes to the FEE where it joins the input to the MR.

6.2.7. *Power converter*

The Power Converter Unit (PCU) supplies all the low-voltage application in the RFES except the ESS-supplied 35 VDC which powers the HPA. A separate spacecraft solid-state power switch turns on the RFES.

6.3. Energy storage subsystem

The Energy Storage Subsystem (ESS) is a battery substitute for the HPA of the RFES, used to reduce the peak-power required by the RADAR during transmission. The ESS does this by boosting the 30 VDC, supplied by the spacecraft, to approximately 80 VDC for storage in a capacitor bank, and then bucks the 80 VDC to 35 VDC for use by the HPA. The boost to 80 VDC is necessary to more effectively store the energy and give some "headroom" so that when the energy is drawn from the capacitor bank the voltage stays above the 35 VDC required. The input to the ESS is limited to 34 W, while the output is approximately 200 W. The RADAR transmits at a $<75\%$ duty cycle for 10–50 ms and then waits for approximately 10 times this interval, until the next transmission occurs. During this "quiet" time the voltage in the ESS builds back up. A separate spacecraft solid-state switch turns on the ESS.

6.4. High gain antenna

Due to volume and mass constraints, the Cassini RADAR uses the spacecraft's high-gain, 4 m diameter telecommunications antenna. To extend the imaging coverage, a multiple radar feed structure at 13.8 GHz is mounted on the antenna reflector to generate five beams. The beams are adjacent to one another in the cross-track dimension, as is shown in Figure 12. The beam configuration is illustrated in Figure 6. In this figure, the central, circular beam (B3) is generated by illuminating the entire

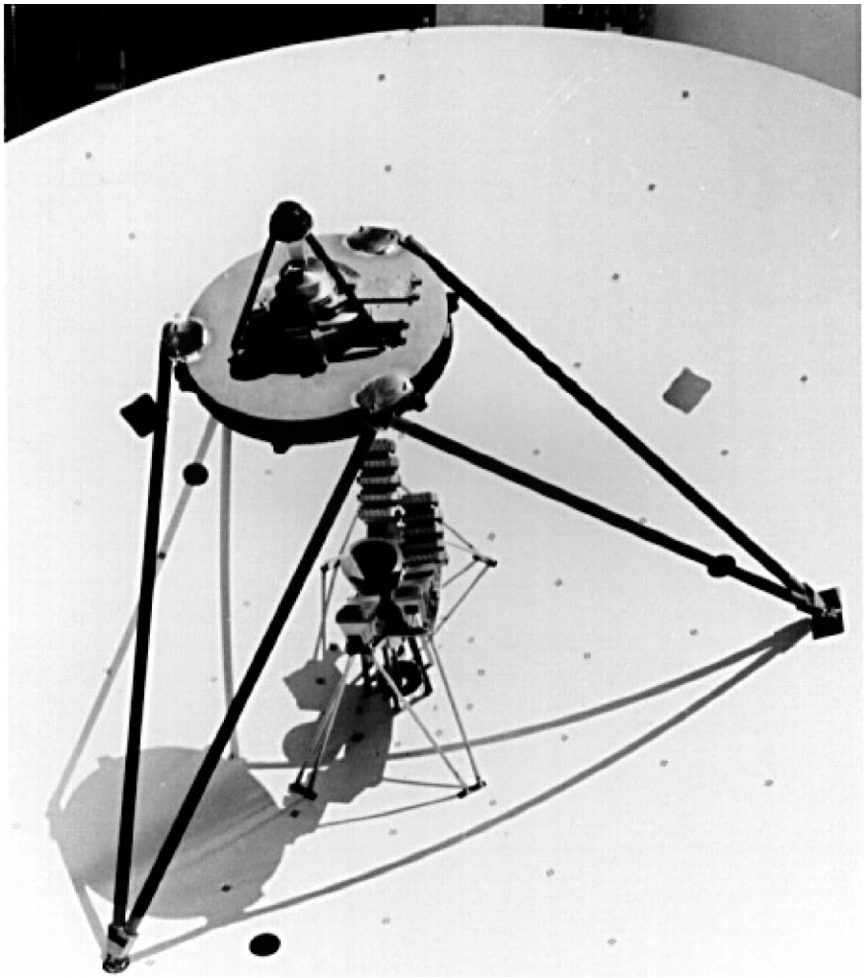

Figure 12. The four-wavelength feed assembly of the Cassini High Gain Antenna. The RADAR Ku-band feeds B1, B2, B4, and B5 are placed–the sides from the antenna's axis.

reflector with a feed that is located at reflector's focal point, and the side-looking beams are generated by partially illuminating the reflector with four feeds that are located away from the focal axis. The expected performance characteristics of the five antenna beams of the Cassini RADAR are given in Table V. During operation, only one beam will be utilized during a radar burst, from 90 to 3,000 ms.

7. Summary

The RADAR experiment will provide a comprehensive set of data that will allow a significant enhancement of our understanding of the present state and evolution of

TABLE V
Cassini RADAR Antenna Performance Characteristics

	Peak gain (dB)	Azimuth beamwidth (°)	Cross-track beamwidth (°)	Angle from focal axis (°)	Peak sidelobe (dB)	Peak cross-pol (dB)
Beams 1 and 5	42.0	0.35	1.35	2.2	−12	−20
Beams 2 and 4	42.1	0.35	1.35	0.85	−13	−20
Beam 3	49.1	0.35	1.35	0	−16	−20

the surface of Titan, by acquiring global radiometric maps and high-to-moderate resolution imaging of about 25% of the moon's surface. The RADAR sensor was designed to have flexibility to respond to a wide range of the presently unknown surface characteristics. As we acquire the first set of data, during the first flybys of Titan, the RADAR sensor configuration and parameters will be reset to optimize the science yield of the data acquired during the subsequent flybys. By the end of the Cassini mission, the RADAR will have provided significant imaging coverage of the last major body in the solar system save the still unmapped Pluto/Charon.

Acknowledgements

We acknowledge the contributions made by the Cassini RADAR Instrument Development Teams both at Alenia Aerospazio and at JPL, and we also acknowledge the support from the Cassini Program. The Alenia portion of the work was carried out under the sponsorship of the Italian Space Agency (ASI); the JPL portion was performed under contract with National Aeronautics and Space Administration (NASA).

References

Allison, M., Godfrey, D. A., and Beebe, R. F.: 1990, 'A wave dynamical interpretation of Saturn's polar hexagon', *Science* **247**, 1061–1063.

Allison, M., Del Genio, A. D., and Zhou, W.: 1995, 'Richardson number constraints for the Jupiter and outer planet wind regime', *Geophys. Res. Lett.* **22**, 2957–2960.

Caldwell, J., Cunningham, C. C., Anthony, D., White, P. H., Groth, E. J., Hassan, H., Noll, K., Smith, P. H., Tomasko, M. G., and Weaver, H. A.: 1992, 'Titan: Evidence for seasonal change—a comparison of Hubble Space Telescope and Voyager images', *Icarus* **96**, 1–9.

Campbell, D. B., Head, J. W., Harmon, J. K., and Hine, A. A.: 1983, 'Venus: Identification of banded terrain in the mountains of Ishtar Terra', *Science* **221**, 644–647.

Downs, G. S., Reichley, P. E., and Green, R. R.: 1975, 'Radar measurements of Martian topography and surface properties: The 1971 and 1973 oppositions', *Icarus* **26**, 273–312.

1070 Dubouloz, N., Raulin, F., Lellouch, E., and Gautier, D.: 1989, 'Titan's hypothesized ocean properties:
1071 The influence of surface temperature and atmospheric composition uncertainties', *Icarus* **82**,
1072 81–96.
1073 Elachi, C.: 1987, *Introduction to the Physics and Techniques of Remote Sensing*, New York: Wiley.
1074 Elachi, C.: 1988, *Spaceborne Radar Remote Sensing: Applications and Techniques*, New York: IEEE
1075 Press.
1076 Elachi, C., Im, E., Roth, L. E., and Werner, C. L.: 1991, 'Cassini Titan Radar Mapper', *Proc. IEEE*
1077 **79**, 867–880.
1078 Engel, S., Lunine, J. I., and Hartmann, W. K.: 1995, 'Cratering on Titan and implications for Titan's
1079 atmospheric history', *Planet. Space Sci.* **43**, 1059–1066.
1080 Ford, P. G., and Pettengill, G. H.: 1992, 'Venus topography and kilometer-scale slopes', *J. Geophys.*
1081 *Res.* **97**, 13,103–13,114.
1082 Griffith, C. A.: 1993, 'Evidence for surface heterogeneity on Titan', *Nature* **364**, 511–514.
1083 Griffith, C. A., Owen, T., and Wagener, R.: 1991, 'Titan's surface and troposphere, investigated with
1084 ground-based, near-infrared observation', *Icarus* **93**, 362–378.
1085 Grossman, A. W.: 1990, 'Microwave imaging of Saturn's deep atmosphere and rings', Doctoral
1086 Dissertation, California Institute of Technology.
1087 Grossman, A. W., and Muhleman, D. O.: 1992, 'Observation of Titan's radio light-curve at 3.5-cm',
1088 *Bull. Am. Astron. Soc.* **24**, 954.
1089 Grossman, A. W., Muhleman, D. O., and Berge, G. L.: 1989, 'High-resolution microwave imaging
1090 of Saturn', *Science* **245**, 1211–1215.
1091 Harmon, J. K., and Ostro, S.J.: 1985, 'Mars: Dual-polarization radar observations with extended
1092 coverage', *Icarus* **62**(1985), 110–128.
1093 Hensley, S., and Im, E.: 1993, 'SAR ambiguity study for the Cassini Radar', *Proceedings of*
1094 *IGARSS'93*.
1095 Hubbard, W. B., and 45 others: 1993, 'The occultation of 28 Sgr by Titan', *Astron. Astrophys.* **269**,
1096 541–563.
1097 Im, E., Johnson, W. T. K., and Hensley, S.: 1993, 'Cassini Radar for remote sensing of Titan - design
1098 considerations', *Proceedings of IGARSS'93*.
1099 Inge, J. L., and Batson, R.M.: 1992, 'Indexes of maps of the planets and satellites', *NASA TM* **4395**,
1100 96–98.
1101 Johnson, W. T. K.: 1991, 'Magellan imaging radar mission to Venus', *Proc. IEEE* **79**, 777.
1102 Kuiper, G. P.: 1944, 'Titan: A satellite with an atmosphere', *Astrophys. J.* **100**, 378–383.
1103 Kwok, R., and Johnson, W. T. K.: 1989, 'Block adaptive quantization of Magellan SAR data', *IEEE*
1104 *Trans. Geosci. Remote Sens.* **27**, 375–383.
1105 Lemmon, M. T., Karkoscka, E., and Tomasko, M.: 1993, 'Titan's rotation: Surface feature observed',
1106 *Icarus* **103**, 329–332.
1107 Lemmon, M. T., Karkoscka, E., and Tomasko, M.: 1995, 'Titan's rotational light-curve', *Icarus* **113**,
1108 27–38.
1109 Lindal, G. F., Wood, G. E., Hotz, H. B., Sweetnam, D. N., Eshleman, V. R., and Tyler, G. L.: 1983,
1110 'The atmosphere of Titan: An analysis of the Voyager 1 radio occultation measurements', *Icarus*
1111 **53**, 348–363.
1112 Lorenz, R. D.: 1995a, 'Raindrops on Titan', *Adv. Space Res.* **15**, (3)317–(3)320.
1113 Lorenz, R. D.: 1995b, 'Cassini mission: Radar sensing of craters on Titan', *Lunar Planet. Sci.* **XXVI**,
1114 775–776.
1115 Lorenz, R. D., and Lunine, J. I.: 1996, 'Erosion on Titan: Past and present', *Icarus* **122**, 79–
1116 91.
1117 Lorenz, R. D., Smith, P. H., Lemmon, M. T., Karkoschka, E., Lockwood, G. W., and Caldwell, J.:
1118 1997, 'Titan's north-south asymmetry from HST and Voyager imaging: Comparison with models
1119 and ground-based photometry', *Icarus* **127**, 173–189.

Lunine, J. I.: 1993. 'Does Titan have an ocean? A review of current understanding of Titan's surface', *Revs. Geophys.* **31**, 133–149.

Lunine, J. I., and Rizk, B.: 1989, 'Thermal evolution of Titan's atmosphere', *Icarus* **80**, 370–389.

Lunine, J. I., Stevenson, D. J., and Yung, Y. L.: 1983, 'Ethane ocean on Titan', *Science* **222**, 1229–1230.

Mitchell, D. L., Ostro, S. J., Hudson, R. S., Rosema, K. D., Campbell, D. B., Vélez, R., Chandler, J. F., Shapiro, I. I., Giorgini, J. F., and Yeomans D. K.: 1996, 'Radar observations of asteroids 1 Ceres, 2 Pallas, and 4 Vesta', *Icarus* **124**, 113–133.

Muhleman, D. O., Grossman, A. W., Butler, B. J., and Slade, M. A.: 1990, 'Radar reflectivity of Titan', *Science* **248**, 975–980.

Muhleman, D. O., Grossman, A. W., Slade, M. A., and Butler, B. J.: 1992, 'The surface of Titan and Titan's rotation: What is radar telling us?', *Bull. Am. Astron. Soc.* **24**, 954.

Muhleman, D. O., Grossman, A. W., Slade, M. A., and Butler, B. J.: 1993, 'Titan's radar reflectivity and rotation', *Bull. Am. Astron. Soc.* **25**, 1009.

Muhleman, D. O., Grossman, A. W., and Butler, B. J.: 1995, 'Radar investigation of Mars, Mercury, and Titan', *Annu. Rev. Earth Planet. Sci.* **23**, 337–374.

Ostro, S. J.: 1993, 'Planetary Radar Astronomy', *Revs. Mod. Phys.* **65**, 1235–1279.

Ostro, S. J., Campbell, D. B., Simpson, R. A., Hudson, R. S., Chandler, J. F., Rosema, K. D., Shapiro, I. I., Standish, E. M., Winkler, R., Yeomans, D. K., Vélez, R., and Goldstein, R. M.: 1992, 'Europa, Ganymede, and Callisto: New radar results from Arecibo and Goldstone', *J. Geophys. Res.* **97**, 18,227–18,244.

Pettengill, G. H.: 31978, 'Physical properties of the planets and satellites from radar observations', *Ann. Rev. Astron. Astrophys.* **16**, 265–292.

Pettengill, G. H., Briscoe, H. W., Evans, J. V., Gehrels, E., Hyde, G. M., Kraft, L. G., Price, R., and Smith, W. B.: 1962, 'A radar investigetion of Venus', *Astron. J.* **67**, 181–190.

Pettengill, G. H., Ford, P. G., Johnson, W. T. K., Raney, K. R., and Soderblom, L. A.: 1991, 'Magellan: Radar performance and data products', *Science* **252**, 260–265.

Samuelson, R. E., and Mayo, L. A.: 1997, 'Steady-state model for methane condensation in Titan's troposphere', *Planet. Space Sci.* **45**, 949–958.

Saunders, R. S., and 26 others: 1992, 'The Magellan Mission summary', *J. Geophys. Res.* **97**, 13,067–13,090.

Sen, A. D., Anicich, V. G., and Arakelian, T.: 1992, 'Dielectric constant of liquid alkanes and hydrocarbon mixtures', *J. Phys. D: Appl. Phys.* **25**, 516–521.

Smith, P. H., and Lemmon, M. T.: 1993, 'HST images of Titan', *Bull. Am. Astron. Soc.* **25**, 1105.

Smith, P. H., Lemmon, M. T., Lorenz, R. D., Sromovsky, L. A., Caldwell, J. J., and Allison, M. D.: 1996, 'Titan's surface, revealed by HST images', *Icarus* **119**, 336–349.

Straty, G. C., and Goodwin, R. D.: 1973, 'Dielectric constant and polarizability of saturated and compressed fluid methane', *Cryogenics***13**, 712–715.

Thomson, W. R., and Squyres, S. W.: 1990, 1Titan and other icy satellites: Dielectric properties of constituent materials and implications for radar sounding', *Icarus* **86**, 336–354.

Toon, O. B., McKay, C. P., Courtin, R., and Ackerman, T. P.: 1988, 'Methane rain on Titan', *Icarus* **75**, 255–284.

Tyler, G. L., Eshleman, V. R., Anderson, J. D., Levy, G. S., Lindal, G. F., Wood, G. E., and Croft, T. A.: 1981, 'Radio science investigations of the Saturn system with Voyager 1: Preliminary results', *Science* **212**, 201–206.

Tyler, G. L., Simpson, R. A., Maurer, M. J., and Holman, E.: 1992, 'Scattering properties of the Venusian surface: Preliminary results from Magellan', *J. Geophys. Res.* **97**, 13,115–13,139.

Queries

Q1. Au: Telephone and fax details have been deleted as per the style of the journal. Please check.
Q2. Au: Affiliation no. 1 given in the manuscript for the first author has been set as a note under the dagger symbol. Please check.
Q3. Au: Smith et al., 1994 and Smith et al., 1995 are unlinked with references in the list. Please provide complete bibliographic details for these citations or delete them.
Q4. Au: Samuelson, 1997 has been set as Samuelson et al., 1997 to match with that given in the reference list. Please check.
Q5. Au: Units of measurement have been set in SI units style throughout the article as per the guidelines outlined in NIST Reference on Constants, Units and Uncertainty. Please check for correctness.
Q6. Au: Please provide the definition for the multiple RS.
Q7. Au: Tables I, II, and V have been formatted as per style. N/A has been defined in the footnote in Tables I and II. Please check for correctness.
Q8. Au: The first sentence in this paragraph been slightly reformatted. Please check for retention of the original sense intended.
Q9. Au: The term 16k has been set as 16K conforming to the upper case K used to denote kilo (=1024) in the computer terminology. Please check for correctness.